

ASR: Attention-alike Structural Re-parameterization[♣]

Shanshan Zhong,¹ Zhongzhan Huang,^{*1} Wushao Wen,¹ Jinghui Qin,^{† 2} Liang Lin,¹
¹Sun Yat-Sen University, ²Guangdong University of Technology,
 {zhongshsh5, huangzhzh23}@mail2.sysu.edu.cn, wenwsh@mail.sysu.edu.cn
 scape1989@gmail.com, linliang@ieee.org

Abstract

The structural re-parameterization (SRP) technique is a novel deep learning technique that achieves interconversion between different network architectures through equivalent parameter transformations. This technique enables the mitigation of the extra costs for performance improvement during training, such as parameter size and inference time, through these transformations during inference, and therefore SRP has great potential for industrial and practical applications. The existing SRP methods have successfully considered many commonly used architectures, such as normalizations, pooling methods, multi-branch convolution. However, the widely used self-attention modules cannot be directly implemented by SRP due to these modules usually act on the backbone network in a multiplicative manner and the modules' output is input-dependent during inference, which limits the application scenarios of SRP. In this paper, we conduct extensive experiments from a statistical perspective and discover an interesting phenomenon *Stripe Observation*, which reveals that channel attention values quickly approach some constant vectors during training. This observation inspires us to propose a simple-yet-effective attention-alike structural re-parameterization (ASR) that allows us to achieve SRP for a given network while enjoying the effectiveness of the self-attention mechanism. Extensive experiments conducted on several standard benchmarks demonstrate the effectiveness of ASR in generally improving the performance of existing backbone networks, self-attention modules, and SRP methods without any elaborated model crafting. We also analyze the limitations and provide experimental or theoretical evidence for the strong robustness of the proposed ASR.

1. Introduction

The structural re-parameterization (SRP) technique [9, 10, 23, 56, 17, 2] is an efficient neural network technology

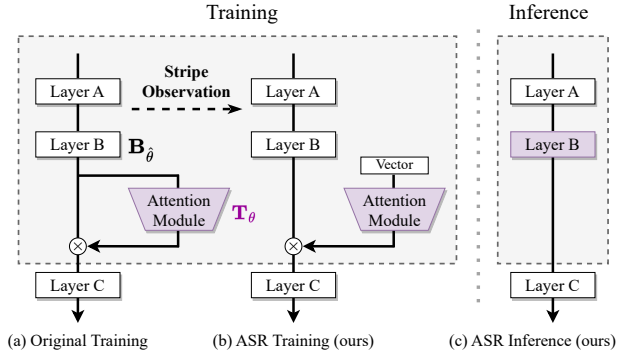


Figure 1. The sketch of ASR. Inspired by *Stripe Observation*, we utilize a learnable vector as input to the attention module for training. In the Inference phase, the attention module can be merged into the parameters of the backbone network.

that decouples training and inference, greatly facilitating the deployment of Deep Neural Networks (DNNs) in practical applications and possessing excellent potential for industrial implementation. During the training phase, for a given backbone network, SRP increases the model's representation power by adding multiple branches or specific layers with various neural network components to the backbone. During the inference phase, the added branches or layers can be merged into the parameters of the backbone network through some equivalent transformations, enabling significant performance improvement without any additional parameters or computational costs. Specifically, for an input x , a branch layer T_θ with learnable parameters θ , and a layer on the backbone $B_{\hat{\theta}}$ (usually a convolutional filter with a sufficiently large kernel size [9]), if there are transformations h and g such that

$$\underbrace{h[T_\theta, B_{\hat{\theta}}]}_{\text{Training}}(x) = \underbrace{B_{g[\hat{\theta}, \theta]}}_{\text{Inference}}(x), \quad (1)$$

this situation can be decoupled in training and inference processing using SRP. For example, during training, $\text{Conv}_\theta(x) + \text{Conv}_{\hat{\theta}}(x)$ can be equivalently transformed into $\text{Conv}_{\theta+\hat{\theta}}(x)$ during inference, enabling the model per-

^{*}Co-first author; [†] Corresponding author; [♣] Technical report

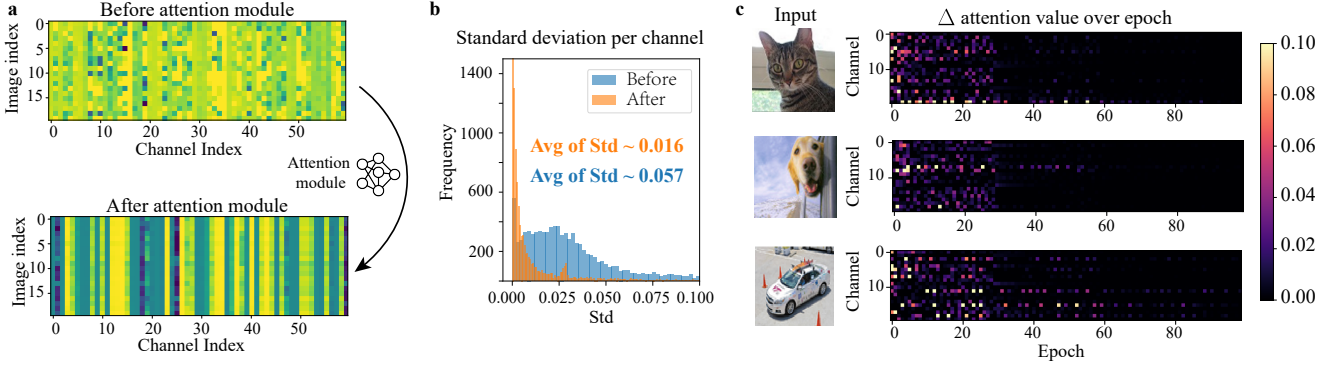


Figure 2. The empirical visualization of the *Stripe Observation*. **a**, after passing through the attention model, the attention values of different images tend to approach a certain value within the same channel, resulting in a “stripe structure”. **b**, the standard deviation of attention values for each channel is almost distributed around zero. **c**, the visualization of the first-order difference (absolute value) for attention value over epoch. Most of the values approach a constant rapidly. Zoom in for best view.

formance of two convolutional filters to be achieved with only one convolutional filter. Another example about batch normalization (BN) is $\text{BN}_\theta(\text{Conv}_\theta(x))$ can be equivalently transformed into $\text{Conv}_{\hat{\theta},a,b}(x)$ during inference, where a and b are constants related to θ . Based on the idea of Eq.(1), although previous SRP methods have successfully integrated various neural network components, including normalization methods, multi-branch convolution, global pooling, etc., existing methods are currently unable to integrate self-attention modules, which are widely used in deep learning applications. This is due to the fact that the self-attention module \mathbf{T}_θ , as illustrated in Fig.1 (a), acts on the backbone network in a multiplicative manner (usually is the element-wise multiplication \odot), and the module’s output is also input-dependent during inference. As these reasons, usually, for a given transformation g , we have

$$\mathbf{B}_{\hat{\theta}} \odot \mathbf{T}_\theta \neq \mathbf{B}_{g[\hat{\theta},\theta]}. \quad (2)$$

The Eq.(2) reveals that the self-attention module is not directly compatible with the existing SRP’s paradigm, which means that the widely used self-attention networks may limit the scenario and scope of SRP. Therefore, there is a question: Can we incorporate the effectiveness of self-attention mechanisms into SRP in an indirect way? To answer this question, we first propose an interesting phenomenon that occurs in different datasets, network structures, and channel attention modules, that is

(Stripe Observation) As shown in Fig.2, the attention value $\mathbf{v}_i \in \mathbb{R}^c$ obtained by i -th channel attention module will rapidly approach to a value $\bar{\mathbf{v}}_i \in \mathbb{R}^c$, which $\bar{\mathbf{v}}_i$ may follow a distribution with mean vector μ_i and covariance matrix $\text{diag}(\sigma_{i1}^2, \dots, \sigma_{ic}^2)$, $\sigma_{ij}, j = 1, 2, \dots, c$ closes to 0.

Empirically, as shown in Fig.2, we visualize the attention values of the well-known attention module SE [22] on the ResNet50 [18] architecture trained on the ImageNet [44]

dataset to observe the so-called *Stripe Observation*. For Fig.2 a, first, we randomly select 20 images from the ImageNet dataset as inputs to the model and visualize the values of feature maps before and after passing through the attention module, where we only show 60 channels randomly selected from all channels. We find that before inputting into the attention module, the values of the feature maps varied greatly among different channels and images, whereas after passing through the module, the values of different images tended to approach a certain value within the same channel, resulting in a “stripe structure”. This is the reason why we refer to this phenomenon as the *Stripe Observation*. Further, we can quantify this observation from a statistical perspective. Specifically, we visualize the standard deviation of values for each channel of the feature map before and after passing through the attention modules, as shown in Fig.2 b. We observe that the standard deviation of values for each channel is almost distributed around zero after passing through the attention module, regardless of the images, indicating that the attention values at any module do indeed approach a corresponding constant vector. Let \mathbf{v}_i^t be the attention value obtained by the i -th module during the t -th epoch, We can further explore the process of forming these constant vectors. Fig.2 c visualizes the first-order difference (absolute value) of three input images over epoch for randomly selected 20 channels, i.e., $\Delta_i = \text{abs}[\mathbf{v}_i^{t+1} - \mathbf{v}_i^t]$. Typically, a commonly used schedule learning rate is applied for training ResNet50 on the ImageNet dataset, where the learning rate is reduced by 90% every 30 epochs. As shown in Fig.2 c, most of the values almost converge at the first learning rate decay (30 epochs), i.e., the first-order difference is zero (black color). More empirical visualizations about *Stripe Observation* can be found in the appendix.

Inspired by the *Stripe Observation* that the channel attention values of different inputs in a dataset tend to approach a constant vector, we propose an Attention-alike Structural

Re-parameterization (ASR) as shown in Fig.1 (b), where we directly consider a learnable vector as the input to the attention modules. This makes the attention modules relatively independent of the model input so that the “attention values” become a constant vector after training. Therefore, the dilemma mentioned in Eq.(2) is solved, and we can achieve the SRP, like Fig.1 (c), of a given model while enjoying the effectiveness of the self-attention mechanism. The details of ASR can be found in Section 3; we also demonstrate the effectiveness of ASR and its compatibility with existing neural network training methods using multiple benchmarks in Section 4. Furthermore, we provide the empirical and theoretical evidences for the strong robustness of ASR in Section 6. We summarize the contributions as follows:

- We revisit the channel attention mechanism from a statistical perspective. With comprehensive experiments, we find the *Stripe Observation*, which reveals that the attention value tends to rapidly approach some constant vectors during training.
- We coin a novel structural re-parameterization method, called ASR, tailored for *Stripe Observation*, which can leverage various attention modules to improve the model performance without extra parameters and inference time.
- We also analyze the limitations and provide experimental or theoretical evidence for the compatibility, effectiveness, and robustness of the proposed ASR.

2. Related works

Self-attention mechanism selectively focuses on the most informative components of a network via self-information processing and has gained a promising performance on vision tasks [35]. For example, SENet [22] proposes the channel attention mechanism, which adjusts the feature map with channel view, and CBAM [58] considers both channel and spatial attention for adaptive feature refinement. Recently, more works [21, 58, 53, 41, 12, 43, 19, 68, 15, 57, 1, 34, 3, 63, 42, 33] are proposed to optimize spatial attention and channel attention. Specifically, ECANet [55] introduces one-dimensional convolution layers to reduce the redundancy of fully connected layers and obtain more efficient results. Besides, considering the pooling method, SRM [32] propose to use GAP with global standard deviation pooling, and SPA [16] introduces a spatial pyramid structure to encode the intermediate features instead of using the simple global average pooling. In particular, IE [26, 35] use a simple pair of learnable parameters instead of convolution or fully connected networks to construct channel attention modules. Most of the above works regard the self-attention mechanism as an additional module of the backbone network, and with the development of the transformer [52], a large number of works [61, 11, 50, 62, 49]

regard the attention as a part of the backbone network, and play a huge role in various fields of artificial intelligence.

Structural re-parameterization enables different architectures to be mutually converted through the equivalent transformation of parameters [23]. For instance, a branch of 1×1 convolution and a branch of 3×3 convolution can be transferred into a single branch of 3×3 convolution [10]. In the training phase, multi-branch [9, 10] and multi-layer [17, 2] topologies are designed to replace the vanilla layers for augmenting models. Afterward, during inference, the training-time complex models are transferred to simple ones for faster inference. Cao et al [2] have discussed how to merge a depthwise separable convolution kernel during training. Thanks to the efficiency of structural re-parameterization, it has gained great importance and has been utilized in various tasks [24, 14, 48, 40, 45, 37, 67, 65] such as compact model design [11], architecture search [4, 64], pruning [7], image recognition [8], and super-resolution [56, 13].

3. Proposed method

Our attention-alike structural re-parameterization (ASR) is a simple-yet-effective method without introducing additional inference-time cost and parameters in inference, which can share the effectiveness of any channel attention module by considering a learnable vector as input for the module. Fig. 1 depicts the sketch of ASR. In the following subsections, we first introduce the preliminary channel attention modules in Section 3.1. We then detail discuss the training and inference phase of ASR in Section 3.2.

3.1. Preliminary: channel attention in vision

Given a single input $\mathbf{x} \in \mathbb{R}^{C \times H \times W}$ of channel attention modules (see Fig.1), we usually obtain the corresponding global information $\mathbf{u} \in \mathbb{R}^{C \times 1 \times 1}$ through global average pooling (GAP) follow [22, 28, 66], where the c -th element of \mathbf{u} is calculated as follows:

$$\mathbf{u}_c = \text{GAP}(\mathbf{x}_c) = \frac{1}{H \times W} \sum_{i=1}^H \sum_{j=1}^W \mathbf{x}_{c,i,j}. \quad (3)$$

Then the attention value $\mathbf{v} \in \mathbb{R}^{C \times 1 \times 1}$ is calculated and leveraged to adjust the input \mathbf{x} using Eq.(4).

$$\mathbf{x}' = \mathbf{x} \odot \mathbf{v}, \text{ where } \mathbf{v} = \mathbf{T}_{\theta}(\mathbf{u}) = \sigma(\mathcal{F}_{\theta}(\mathbf{u})), \quad (4)$$

where \odot denotes channel-wise multiplication, \mathcal{F}_{θ} is the neural network part of self-attention modules with learnable parameters θ , and $\sigma(\cdot)$ is Sigmoid activation function.

3.2. Attention-alike structural re-parameterization

Training phase. Based on *Stripe Observation*, we can directly consider a learnable vector $\psi \in \mathbb{R}^{C \times 1 \times 1}$ as the input of \mathcal{F}_{θ} . Without GAP, we measure the output of attention

Backbone	Module	STL10		CIFAR100		CIFAR10	
		Top-1 acc.	Top-5 acc.	Top-1 acc.	Top-5 acc.	Top-1 acc.	Top-5 acc.
ResNet164	-	82.38	98.75	74.32	93.21	92.97	99.72
	ASR (SE)	83.70 ($\uparrow 1.32$)	99.10 ($\uparrow 0.35$)	75.36 ($\uparrow 1.04$)	93.53 ($\uparrow 0.32$)	94.47 ($\uparrow 1.50$)	99.77 ($\uparrow 0.05$)
	ASR (IE)	85.15 ($\uparrow 2.77$)	98.60 ($\downarrow -0.15$)	75.58 ($\uparrow 1.26$)	93.84 ($\uparrow 0.63$)	94.39 ($\uparrow 1.42$)	99.83 ($\uparrow 0.11$)
	ASR (SRM)	83.76 ($\uparrow 1.38$)	99.09 ($\uparrow 0.34$)	75.23 ($\uparrow 0.91$)	93.68 ($\uparrow 0.47$)	94.45 ($\uparrow 1.48$)	99.90 ($\uparrow 0.18$)
	ASR (SPA)	83.44 ($\uparrow 1.06$)	98.76 ($\uparrow 0.01$)	75.12 ($\uparrow 0.80$)	93.44 ($\uparrow 0.23$)	94.65 ($\uparrow 1.68$)	99.89 ($\uparrow 0.17$)
VGG19	-	79.23	98.09	72.48	89.35	93.15	99.52
	ASR (SE)	79.95 ($\uparrow 0.72$)	98.34 ($\uparrow 0.25$)	73.37 ($\uparrow 0.89$)	90.15 ($\uparrow 0.80$)	93.98 ($\uparrow 0.83$)	99.71 ($\uparrow 0.19$)
	ASR (IE)	80.48 ($\uparrow 1.25$)	98.36 ($\uparrow 0.27$)	73.41 ($\uparrow 0.93$)	89.90 ($\uparrow 0.55$)	93.55 ($\uparrow 0.40$)	99.60 ($\uparrow 0.08$)
	ASR (SRM)	80.35 ($\uparrow 1.12$)	98.54 ($\uparrow 0.45$)	73.33 ($\uparrow 0.85$)	90.08 ($\uparrow 0.73$)	93.60 ($\uparrow 0.45$)	99.64 ($\uparrow 0.12$)
	ASR (SPA)	80.23 ($\uparrow 1.00$)	98.44 ($\uparrow 0.35$)	73.38 ($\uparrow 0.90$)	90.13 ($\uparrow 0.78$)	93.79 ($\uparrow 0.64$)	99.64 ($\uparrow 0.12$)
ShuffleNetV2	-	80.34	98.93	71.12	91.55	91.68	99.69
	ASR (SE)	81.46 ($\uparrow 1.12$)	98.95 ($\uparrow 0.02$)	71.34 ($\uparrow 0.22$)	92.58 ($\uparrow 1.03$)	91.68 ($\uparrow 0.00$)	99.75 ($\uparrow 0.06$)
	ASR (IE)	82.83 ($\uparrow 2.49$)	98.94 ($\uparrow 0.01$)	71.89 ($\uparrow 0.77$)	92.51 ($\uparrow 0.96$)	91.90 ($\uparrow 0.22$)	99.77 ($\uparrow 0.08$)
	ASR (SRM)	81.28 ($\uparrow 0.94$)	98.99 ($\uparrow 0.06$)	71.79 ($\uparrow 0.67$)	92.77 ($\uparrow 1.22$)	91.69 ($\uparrow 0.01$)	99.75 ($\uparrow 0.06$)
	ASR (SPA)	82.15 ($\uparrow 1.81$)	99.00 ($\uparrow 0.07$)	72.05 ($\uparrow 0.93$)	92.75 ($\uparrow 1.20$)	91.71 ($\uparrow 0.03$)	99.80 ($\uparrow 0.11$)
MobileNet	-	80.35	98.44	66.87	89.74	90.97	99.69
	ASR (SE)	81.18 ($\uparrow 0.83$)	98.66 ($\uparrow 0.22$)	68.91 ($\uparrow 2.04$)	90.06 ($\uparrow 0.32$)	91.48 ($\uparrow 0.51$)	99.75 ($\uparrow 0.06$)
	ASR (IE)	81.38 ($\uparrow 1.03$)	98.45 ($\uparrow 0.01$)	69.45 ($\uparrow 2.58$)	89.68 ($\downarrow -0.06$)	91.30 ($\uparrow 0.33$)	99.78 ($\uparrow 0.09$)
	ASR (SRM)	81.51 ($\uparrow 1.16$)	98.38 ($\downarrow -0.06$)	69.04 ($\uparrow 2.17$)	90.39 ($\uparrow 0.65$)	91.09 ($\uparrow 0.12$)	99.69 ($\uparrow 0.00$)
	ASR (SPA)	81.35 ($\uparrow 1.00$)	98.41 ($\downarrow -0.03$)	68.56 ($\uparrow 1.69$)	90.81 ($\uparrow 1.07$)	91.36 ($\uparrow 0.39$)	99.63 ($\downarrow -0.06$)
ViT [†]	-	61.49	96.15	66.63	86.29	89.00	99.17
	ASR (SE)	65.39 ($\uparrow 3.90$)	96.98 ($\uparrow 0.83$)	67.82 ($\uparrow 1.19$)	87.80 ($\uparrow 1.51$)	89.69 ($\uparrow 0.69$)	99.42 ($\uparrow 0.25$)
	ASR (IE)	64.54 ($\uparrow 3.05$)	96.79 ($\uparrow 0.64$)	67.45 ($\uparrow 0.82$)	87.23 ($\uparrow 0.94$)	89.63 ($\uparrow 0.63$)	99.36 ($\uparrow 0.19$)
	ASR (SRM)	62.61 ($\uparrow 1.12$)	96.31 ($\uparrow 0.16$)	68.12 ($\uparrow 1.49$)	87.80 ($\uparrow 1.51$)	89.96 ($\uparrow 0.96$)	99.27 ($\uparrow 0.10$)
	ASR (SPA)	64.38 ($\uparrow 2.89$)	96.71 ($\uparrow 0.56$)	68.41 ($\uparrow 1.78$)	87.92 ($\uparrow 1.63$)	89.88 ($\uparrow 0.88$)	99.24 ($\uparrow 0.07$)

Table 1. The accuracy (%) of ASR for various vision backbones on STL10, CIFAR100, and CIFAR10. [†] All the experimental results of ViT are training from scratch and the details of training settings can be found in the appendix.

modules by $\mathbf{v}_{\psi,\theta} = \sigma(\mathcal{F}_{\theta}(\psi)) \in \mathbb{R}^{C \times 1 \times 1}$. Then during the training phase, ψ will be simultaneously updated with other learnable parameters.

Inference phase. After training, according to the paradigm of SRP, we consider equivalently merging the attention module into the backbone, as shown in Fig. 1 (c). Since the “attention value” $\mathbf{v}_{\psi,\theta}$ is a constant vector, for the various common-used modules $\mathbf{B}_{\hat{\theta}}$ in backbone, we can seamlessly find the corresponding transformation g such that

$$\mathbf{B}_{\hat{\theta}} \odot \mathbf{v}_{\psi,\theta} = \mathbf{B}_{g[\hat{\theta}, \psi, \theta]}, \quad (5)$$

for example, for input \mathbf{x} , if $\mathbf{B}_{\hat{\theta}}$ is a convolutional layer \mathcal{C} with kernels \mathbf{K} and bias \mathbf{b} , then Eq.(5) can be rewritten as

$$\begin{aligned} \mathcal{C}(\mathbf{x}; \mathbf{K}, \mathbf{b}) \odot \mathbf{v}_{\psi,\theta} &= \mathbf{x} * \mathbf{K} \odot \mathbf{v}_{\psi,\theta} + \mathbf{b} \odot \mathbf{v}_{\psi,\theta} \\ &= \mathcal{C}(\mathbf{x}; \mathbf{K} \odot \mathbf{v}_{\psi,\theta}, \mathbf{b} \odot \mathbf{v}_{\psi,\theta}), \end{aligned} \quad (6)$$

where $*$ denote convolution and $\mathbf{K} \odot \mathbf{v}_{\psi,\theta}$ means that the the product of i -th elements of $\mathbf{v}_{\psi,\theta}$ and i -th kernel of \mathbf{K} . Since the existing SRP methods mainly merge various neural network layers into a convolutional layer, from Eq.(6), ASR is compatible with most of these SRP methods. Moreover, since the channel attention module is generally placed after the normalization layer, we can also take batch nor-

malization BN as an example, i.e.,

$$\begin{aligned} \mathbf{BN}(\mathbf{x}; \gamma, \beta) \odot \mathbf{v}_{\psi,\theta} &= \frac{(\mathbf{x} - \mu) \odot \gamma \odot \mathbf{v}_{\psi,\theta}}{\sigma} + \beta \odot \mathbf{v}_{\psi,\theta} \\ &= \mathbf{BN}(\mathbf{x}; \gamma \odot \mathbf{v}_{\psi,\theta}, \beta \odot \mathbf{v}_{\psi,\theta}), \end{aligned} \quad (7)$$

where μ, σ, γ , and β are the accumulated mean, standard deviation, and learned scaling factor and bias of BN, respectively. The equivalent transformations for other $\mathbf{B}_{\hat{\theta}}$, including fully connected layers, transformer-based attention network, etc., can be found in the appendix.

Module	ResNet18	ResNet34	ResNet50
Org	69.75	73.31	76.13
ASR (SE)	70.14 ($\uparrow 0.39$)	74.04 ($\uparrow 0.73$)	76.70 ($\uparrow 0.57$)
ASR (CBAM)	70.29 ($\uparrow 0.54$)	74.00 ($\uparrow 0.69$)	76.68 ($\uparrow 0.55$)
ASR (ECA)	70.30 ($\uparrow 0.55$)	73.88 ($\uparrow 0.57$)	76.87 ($\uparrow 0.74$)
ASR (SRM)	70.08 ($\uparrow 0.33$)	73.96 ($\uparrow 0.65$)	76.55 ($\uparrow 0.42$)

Table 2. Top-1 accuracy (%) of ASR on ImageNet. “Org” means vanilla DNNs.

4. Experiments

4.1. Implementation details

In our study, we employ various backbone architectures, including vanilla ResNet [18], VGG [47], ShuffleNetV2 [39], MobileNet [20], ViT [11], RepVGG [10],

Model	STL10	CIFAR100
RepVGGA0	83.48	68.80
RepVGGA0-ASR (SE)	84.01 ($\uparrow 0.53$)	69.38 ($\uparrow 0.58$)
RepVGGB3	87.05	76.70
RepVGGB3-ASR (SE)	88.29 ($\uparrow 1.24$)	77.42 ($\uparrow 0.72$)
ResNet56 [‡]	82.25	70.67
ResNet56-ACNet	83.11 ($\uparrow 0.86$)	71.42 ($\uparrow 0.75$)
ResNet56-ACNet-ASR (SE)	84.79 ($\uparrow 2.54$)	71.81 ($\uparrow 1.14$)
ResNet110 [‡]	82.02	72.60
ResNet110-ACNet	83.54 ($\uparrow 1.52$)	73.01 ($\uparrow 0.41$)
ResNet110-ACNet-ASR (SE)	86.13 ($\uparrow 4.11$)	73.46 ($\uparrow 0.86$)
ResNet164 [‡]	81.78	71.24
ResNet164-ACNet	83.91 ($\uparrow 2.13$)	71.60 ($\uparrow 0.36$)
ResNet164-ACNet-ASR (SE)	84.65 ($\uparrow 2.87$)	73.50 ($\uparrow 2.26$)

Table 3. Top-1 accuracy (%) of ASR (SE) applied to well-known SRP methods RepVGG [10] and ACNet [6]. RepVGGA0 and RepVGGB3 are RepVGG models with different layers of each stage and multipliers[10]. [‡] We follow the settings of ResNet in the official code of ACNet, which have different layers of each stage and design (basic-block) compared to the ResNet in Table 1.

and ResNet-ACNet [6]. Additionally, we use SE [22], CBAM [58], IE [54, 35], SRM [32], ECA [55], and SPA [16] as the attention modules in our experiments. We employ several popular datasets, namely ImageNet [44], STL10 [5], and CIFAR10/100 [31] in our experiments. Additionally, we use COCO [36] in our style transfer experiments. All experiments are performed using at least 3 runs to ensure statistical significance. We provide detailed training recipes in the appendix.

4.2. ASR for various backbones

In this section, we examine the task of image classification to study the capability of ASR applied in popular visual backbones as shown in Table 1 and Table 2. To ensure a fair and intuitive comparison, the experimental settings are the same for the same backbones.

Observations. The experimental results presented in Table 1 indicate that ASR is capable of significantly improving the performance of various backbone models on commonly used datasets, with the maximum improvement being 3.90% in terms of top-1 accuracy. Moreover, ASR is flexible and can be extended to use various attention modules, exhibiting stable performance across different settings. Table 2 demonstrates that ASR also performs well on more challenging datasets such as ImageNet, indicating its potential to be applied to a wider range of computer vision tasks. To demonstrate the performance of ASR and ensure a fair comparison, we adopt a from-scratch training strategy for ViT experiments without pretraining. As a result, its performance is relatively lower than other backbones, consistent with past findings [38, 30]. However, even under such circumstances, the results in Table 1 show the effectiveness of ASR for ViT.

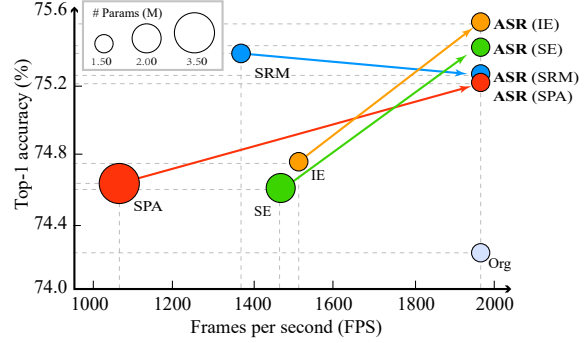


Figure 3. The top-1 accuracy, number of parameters, and the inference speed of various attention modules and corresponding ASR.

Additionally, as an attention-alike method, ASR exhibits performance differences from the original attention modules in terms of accuracy, frames per second (FPS), and parameter count, as shown in Fig. 3. ASR has absolute advantages in terms of FPS and parameter count than attention modules. With an appropriate attention module, ASR can even outperform the attention modules in terms of accuracy. Overall, our experimental results suggest that ASR is a promising approach for enhancing the performance of various vision backbones. In the next section, we will further investigate its compatibility with existing attention modules and SRP methods.

4.3. The compatibility of ASR

ASR for existing attention modules. As shown in Fig. 1, ASR is an attention-like mechanism. It is natural to wonder whether ASR is compatible with DNNs that already incorporate attention modules. To investigate this, we conduct experiments as shown in Table 3.2, and find that ASR significantly improves the performance of DNNs that have attention modules.

ASR for existing SRP methods. We also examine the compatibility of ASR with SRP. Specifically, we select RepVGG [10] and ACNet [6], which utilize SRP in different ways, and evaluated their performance with and without ASR (SE). The results presented in Table 3 indicate that ASR is also highly compatible with SRP, and can further improve the performance of these models.

In summary, the experiments in this section demonstrate that ASR can not only enhance the general visual backbone network by re-parameterization with the given attention modules but also be compatible with existing attention modules and SRP methods. This makes ASR widely applicable in various scenarios.

5. Ablation study

(1) About the position of ASR. In Section 3.2, we mentioned that the constant vectors generated by ASR are not directly related to the input and are applied to the backbone network in a channel-wise multiplication form. There-

Backbone	Module κ	STL10		CIFAR100		CIFAR10	
		Without ASR	With ASR	Without ASR	With ASR	Without ASR	With ASR
ResNet83	SE	84.21	85.51 ($\uparrow 1.30$)	74.62	75.87 ($\uparrow 1.25$)	94.21	94.44 ($\uparrow 0.23$)
	IE	84.03	85.70 ($\uparrow 1.67$)	74.74	75.57 ($\uparrow 0.83$)	94.33	94.45 ($\uparrow 0.12$)
	SRM	82.09	84.83 ($\uparrow 2.74$)	75.38	75.78 ($\uparrow 0.40$)	94.55	94.91 ($\uparrow 0.36$)
	SPA	77.54 [‡]	80.88 ($\uparrow 3.34$)	74.64	74.92 ($\uparrow 0.28$)	94.41	94.65 ($\uparrow 0.24$)
ResNet164	SE	83.81	86.41 ($\uparrow 2.60$)	75.29	77.32 ($\uparrow 2.03$)	94.59	95.09 ($\uparrow 0.50$)
	IE	84.69	85.99 ($\uparrow 1.30$)	75.78	76.20 ($\uparrow 0.42$)	94.06	94.66 ($\uparrow 0.60$)
	SRM	84.85	85.20 ($\uparrow 0.35$)	75.32	77.18 ($\uparrow 1.86$)	94.44	95.26 ($\uparrow 0.82$)
	SPA	75.33 [‡]	79.61 ($\uparrow 4.28$)	75.48	77.25 ($\uparrow 1.77$)	94.83	95.20 ($\uparrow 0.37$)

Table 4. The experiments about the compatibility of ASR for existing attention modules. Given an attention module κ , “Without ASR” means the backbone with only the module κ . “With ASR” denotes the backbone with both κ and ASR (κ). [‡] We have repeated five runs for SPA on STL10. Although its performance is relatively low compared to other modules, it still demonstrates the effectiveness of ASR.

Module	Position	STL10	CIFAR100	CIFAR10
ASR (SE)	(a)	78.31	74.21	93.68
	(b)	80.95	73.77	94.23
	(c) (ours)	83.70	75.36	94.47
	(d)	63.15	39.47	67.68
ASR (IE)	(a)	80.63	73.60	93.83
	(b)	81.65	73.66	83.59
	(c) (ours)	85.15	75.58	94.39
	(d)	62.89	57.76	83.85

Table 5. Top-1 accuracy (%) of ResNet164 with ASR inserted at different positions of the residual block. The **Position** corresponds to the labels in Fig. 4.

fore, theoretically, they can be applied to most positions in the backbone. However, empirical evidence from previous work [27] has revealed that the position of the attention module has a significant impact on the model’s performance. Taking ResNet164 as an example, as shown in Fig. 4, we examine the specific impact of using ASR at four different positions on the model’s performance. The results, as shown in Table 4.3, indicate that using ASR at different positions does have a significant impact on performance. Specifically, using ASR after the batch normalization (BN) yields the best performance, which is consistent with observations from previous works [16, 35, 22] on attention mechanisms. The attention module can effectively adjust the batch noise by BN to improve performance[35]. Moreover, the results in Table 4.3 suggest that using ASR after the ReLU activation function should be chosen with caution, as it may significantly reduce the model’s performance.

Module	$\delta = 1$	$\delta = 2$	$\delta = 3$	$\delta = 4$
ASR (SE)	75.36	75.87	75.72	75.22
ASR (IE)	75.58	75.71	75.45	74.56
ASR (SRM)	75.23	75.45	75.61	75.11
ASR (SPA)	75.12	75.43	75.81	75.62

Table 6. Top-1 accuracy (%) of ResNet164 with different numbers δ of ASR inserted at the same position on CIFAR100. Bold and underline indicate the best results and the second best results, respectively.

(2) About multiple uses of ASR. Since ASR can elim-

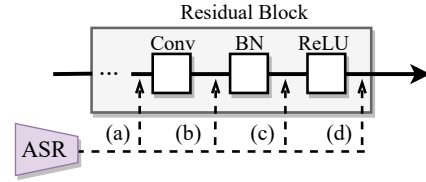


Figure 4. The ablation study about the position for ASR.

inate the extra parameter and inference cost of the attention modules in the backbones during inference, theoretically, there will be no extra cost in the inference stage no matter how many times ASR is used for attention module re-parameterization. Therefore, we investigate the impact of multiple uses of ASR on the model’s performance, denoted as δ . As shown in Table 6, the performance of the model increases first and then decreases with the increase of δ . This phenomenon suggests that ASR can further enhance the performance of the network that has already been trained with ASR, but δ cannot be too large. This is because, in general, the output of the attention module goes through a Sigmoid activation function, whose each value is not large than 1. If δ is too large, the backbone network’s feature map will become small in value due to being multiplied by too many of these vectors, affecting the model’s training and information forwarding. Moreover, when δ is larger, the computational cost of training increases. Therefore, in all experiments in this paper, we generally choose $\delta = 1$.

Module	Ours	$C_{0.1}$	$C_{0.3}$	$C_{0.5}$	$N_{0.1}$	$N_{0.3}$	$N_{0.5}$
ASR (SE)	75.36	75.18	75.09	75.07	74.56	75.02	74.93
ASR (IE)	75.58	75.24	75.11	75.14	75.36	75.17	75.47

Table 7. ResNet164-ASR without learnable input ψ on CIFAR100. C_i and N_i denote the initialization of unlearnable ψ . C_i means that the all elements of ψ are constant i and N_i means that ψ samples from the normal distribution $N(0, i^2 \mathbf{I}_{\dim(\psi)})$.

(3) About the learnable input ψ . We discuss the importance of the learnable input ψ for ASR. From the ASR paradigm, we verify the performance when ψ is a constant C_i or N_i , where C_i means that the all elements of ψ are

constant i and N_i means that ψ samples from the normal distribution $N(\mathbf{0}, i^2 \mathbf{I}_{\dim(\psi)})$. The results are shown in Table 5, where we can find the performance with constant ψ is weaker relative to the learnable one, while the performance seems good when $C_{0.1}$. Therefore, in the experiments of this paper ϕ are initialized with $C_{0.1}$, and results about other initializations can be found in the Appendix.

6. Analysis

(1) Why do attention values approach some constant vectors?

In the introduction, we observe *Stripe Observation* consistently across a wide range of experimental settings. This phenomenon is intriguing and although not easily explained by theory, it appears empirically reasonable. Given a dataset D , certain priors such as location and color priors exist in D and they have a significant impact on neural network learning, especially for attention networks that excel at capturing inductive biases. The attention mechanism adaptively adjusts the weights of feature maps to extract key information and suppress irrelevant information, which can be visualized through Grad-CAM [46]. Specifically, we use the pre-trained SENet [22] and SRMNet [32] as backbones and randomly sample 500 images from the STL10 and ImageNet datasets, and measure the average attention visualizations (using Grad-CAM) of these images under the given backbones, as shown in Fig. 5. We find that the regions of interest identified by the network tend to be biased toward the center of the images in all visualizations. This is because in the shooting or annotation process of these datasets, the target object y was inherently present in the salient location of the image (close to the center), or else the image would not be labeled with the corresponding label of y . Therefore, intuitively, the existence of a series of constant “attention” values that satisfy certain priors of the network is reasonable, and these constant vectors can be regarded as the average embodiment of certain priors in D .

Moreover, despite the fact that according to the *Stripe Observation*, attention values approach to some constant vectors, if we directly replace the attention module with these vectors during the inference phase, taking Table 1 as a baseline, the average performance will decrease by approximately 28%, and there will still be around 15% performance loss even with finetuning. Therefore, our proposed ASR still needs to consider the participation of the attention module during training.

(2) Why does ASR work? ASR generates constant vectors through the attention module to help the training of DNNs, and we find that these constant vectors from ASR can regulate the noise to enhance the robustness of DNNs and help model training.

Theorem 6.1. Consider ASR for a L layers residual neural network with self-attention module $T(\cdot)$, and the corresponding constant input at t -th layer ψ_t , i.e., $x_{t+1} =$

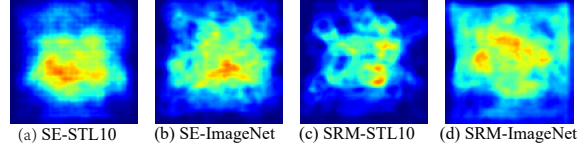


Figure 5. The visualization of average grad-CAM.

$x_t + f(x_t; W_t) \odot T[f(\psi_t)]$, $t = 0, 1, \dots, L - 1$. Let ϵ be the perturbation from the noise and satisfies $\|x_0^\epsilon - x_0\| = \epsilon$, and $\epsilon_t = \|x_t^\epsilon - x_t\|$, we have

$$\epsilon_{t+1} \leq \epsilon_t (1 + \alpha_t \|W_t\|_2), \quad (8)$$

where $\alpha_t = \max\{T[f(\psi_t)]\}$ and \max refers to the largest element in a vector. See proof in the appendix.

Given an input x_0 of the network and a perturbation ϵ , let the noise input x_0^ϵ satisfied $x_0^\epsilon \in \{x \| x - x_0\| = \epsilon\}$. According to Theorem 6.1, for a L layers ResNet, the noise impact $\epsilon_L = \|x_L^\epsilon - x_L\|$ satisfies the following inequation:

$$\epsilon_L \leq \epsilon_{L-1} (1 + \alpha_t \|W_{L-1}\|_2) \leq \epsilon M, \quad (9)$$

where $M = \prod_{t=1}^{L-1} (1 + \alpha_t \|W_t\|_2)$ and it will be a constant in inference phase. Without ASR, i.e., $\alpha_t = 1$, the upper bound of the noise impact ϵ_L increases rapidly with the network depth L due to $(1 + \alpha_t \|W_{L-1}\|_2) \geq 1$. However, with the regulation of ASR, which restricts $0 \leq \alpha_t \leq 1$, this increasing trend of the upper bound can be mitigated, resulting in a robust model. Moreover, since mild noise is generally beneficial to model training, ASR needs to adaptively allow for a moderate amount of noise during training. Additionally, the constant vectors $T[f(\psi_t)]$ generated by ASR cannot be zero vectors, as this would lead to the degradation of the residual network to $x_{t+1} = x_t$, although the upper bound of noise impact ϵ_L could be minimized.

We conduct experiments on three types of noise attacks to empirically verify the ability of ASR in regulating noise to improve model robustness, including batch noise, constant noise, and random noise. We consider the style transfer task, which generally adopts the instance normalization (IN) without batch noise, rather than BN, as adding batch noise would significantly reduce the quality of generated images due to noise interference. As shown in Fig. 6, ASR can significantly alleviate the adverse effects of noise when batch noise is introduced, resulting in image quality comparable to that of IN without batch noise.

Next, we examine constant noise and random noise attacks, following the settings in [35], we inject noise N_a and N_b in each BN layer of ResNet164, i.e., $\text{BN}(\mathbf{x}; \gamma, \beta) = [\frac{x - \mu}{\sigma} \odot N_a + N_b] \odot \gamma + \beta$. For constant noise, N_a and N_b are constant, while $N_a \sim N(1, \sigma_{N_a})$ and $N_b \sim N(0, \sigma_{N_b})$ in random noise scenario. As shown in Table 6, both types of

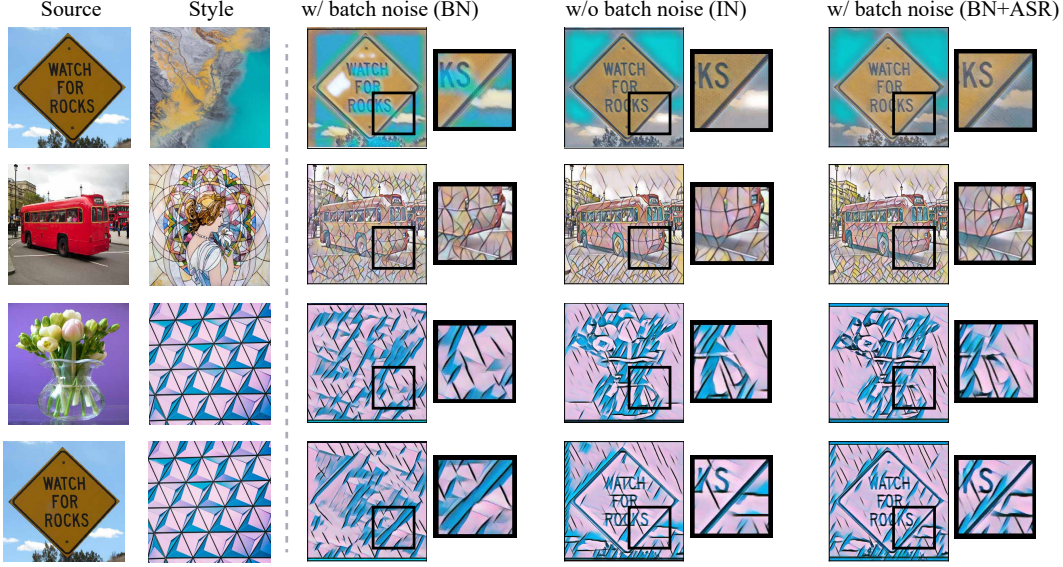


Figure 6. The results about the batch noise attack. Zoom in for best view. See appendix for more results.

(N_a, N_b)	Origin	ASR (SE)	ASR (IE)	ASR (SRM)	ASR (SPA)
(1.0,0.0)	74.32	75.36 ($\uparrow 1.04$)	75.58 ($\uparrow 1.26$)	75.23 ($\uparrow 0.91$)	75.12 ($\uparrow 0.80$)
(0.8,0.8)	45.42	68.81 ($\uparrow 23.39$)	69.85 ($\uparrow 24.43$)	69.57 ($\uparrow 24.15$)	73.48 ($\uparrow 28.06$)
(0.8,0.5)	46.10	71.13 ($\uparrow 25.03$)	72.38 ($\uparrow 26.28$)	71.69 ($\uparrow 25.59$)	73.74 ($\uparrow 27.64$)
(0.5,0.5)	35.77	72.18 ($\uparrow 36.41$)	72.69 ($\uparrow 36.92$)	71.85 ($\uparrow 36.08$)	72.82 ($\uparrow 37.05$)
(0.5,0.2)	73.10	74.48 ($\uparrow 1.38$)	75.36 ($\uparrow 2.26$)	75.02 ($\uparrow 1.92$)	75.07 ($\uparrow 1.97$)
$(\sigma_{N_a}, \sigma_{N_b})$	Origin	ASR (SE)	ASR (IE)	ASR (SRM)	ASR (SPA)
(0.1,0.1)	73.16 \pm 0.26	75.29 \pm 0.13	75.00 \pm 0.79	75.00 \pm 0.12	74.69 \pm 0.16
(0.1,0.2)	73.75 \pm 0.47	74.91 \pm 0.24	74.98 \pm 0.10	75.04 \pm 0.23	74.93 \pm 0.21
(0.2,0.1)	72.63 \pm 0.49	75.15 \pm 0.19	74.85 \pm 0.06	75.22 \pm 0.11	75.03 \pm 0.19

Table 8. Top-1 Accuracy (%) of vanilla ResNet164 (**Origin**) and ASR-enhanced ResNet164 on CIFAR100 under constant or random noise attack. σ refers to the variance of the normal distribution used to generate random noise.

noise have a large impact on neural network training. However, compared with the original network, ASR can significantly mitigate the performance loss suffered by the model, and the performance is more stable, i.e., the variance of top-1 accuracy is smaller.

(3) How to make ASR stronger? Firstly, the attention module in ASR is crucial for performance improvement. We can remove the attention module and only retain a learnable vector as a constant vector needed for ASR inference. The experimental results, as shown in Table 6, indicate that although this approach also leads to some performance improvement, its effectiveness is significantly lower than that of ASR with specific attention modules. Additionally, in the experiments presented in this paper, we find that the performance of ASR is closely related to the selection of attention modules, and different modules exhibit varying performance improvements in various tasks. For instance, as shown in Table 1, for ResNet164, the IE module shows a significant performance advantage, while in ViT, the SE module performs best. These observations imply that the specific modules need to be designed for different scenarios. Since all of ASR can be integrated into the backbone during

the inference phase, researchers can consider more complex and efficient attention modules in the ASR paradigm to meet the needs of different tasks without worrying about the additional parameter load and inference cost generated by the module during inference.

Attention module	STL10	CIFAR100	CIFAR10
-	82.38	74.32	92.97
\times	83.44 ($\uparrow 1.06$)	74.46 ($\uparrow 0.14$)	92.84 ($\downarrow -0.13$)
\checkmark	85.15 ($\uparrow 2.77$)	75.58 ($\uparrow 1.26$)	94.65 ($\uparrow 1.68$)

Table 9. ResNet164-ASR with or without attention modules.

(4) Limitation of proposed ASR. ASR is inspired by the intriguing *Stripe Observation*, which reveals that the channel attention values corresponding to any input in the dataset approach to some constant vectors after neural network training. However, this observation does not hold for other types of attention, including spatial attention and transformer-based attention (see appendix for visualization). These types of attention have individual attention maps for different inputs, which means that ASR may not be directly transferable to their corresponding attention modules. Further details and comparisons can be found in the appendix. Additionally, from an application perspective, although ASR has been validated in multiple classification scenarios, its versatility for other more challenging downstream tasks remains uncertain. Fortunately, in Analysis (3) we suggests that the researchers can design more complex and tailored attention modules to solve these tasks benefited from the flexibility of the ASR paradigm.

7. Conclusion

In this paper, we introduce a novel attention-alike structural re-parameterization (ASR) method, tailored for the channel attention mechanism, which enables effective in-

terconversion between different network architectures. Our discovery of the *Stripe Observation* provides new insights into the channel attention mechanism from a statistical perspective, leading to the development of ASR. Extensive experiments demonstrate that ASR can improve model performance without extra parameters and inference time. We have also provided experimental and theoretical evidence for the compatibility, effectiveness, and robustness of ASR, making it a promising approach for practical applications.

References

- [1] Irwan Bello, Barret Zoph, Ashish Vaswani, Jonathon Shlens, and Quoc V Le. Attention augmented convolutional networks. In *Int. Conf. Comput. Vis.*, pages 3286–3295, 2019. [3](#)
- [2] Jinming Cao, Yangyan Li, Mingchao Sun, Ying Chen, Dani Lischinski, Daniel Cohen-Or, Baoquan Chen, and Changhe Tu. Do-conv: Depthwise over-parameterized convolutional layer. *arXiv 2006.12030*, 2020. [1](#), [3](#)
- [3] Yue Cao, Jiarui Xu, Stephen Lin, Fangyun Wei, and Han Hu. Gcnet: Non-local networks meet squeeze-excitation networks and beyond. In *IEEE Conf. Comput. Vis. Worksh.*, pages 0–0, 2019. [3](#)
- [4] Shoufa Chen, Yunpeng Chen, Shuicheng Yan, and Jiashi Feng. Efficient differentiable neural architecture search with meta kernels. *arXiv 1912.04749*, 2019. [3](#)
- [5] Adam Coates, Andrew Ng, and Honglak Lee. An analysis of single-layer networks in unsupervised feature learning. In *Proceedings of the fourteenth international conference on artificial intelligence and statistics*, pages 215–223. JMLR Workshop and Conference Proceedings, 2011. [5](#)
- [6] Xiaohan Ding, Yuchen Guo, Guiguang Ding, and Jungong Han. Acnet: Strengthening the kernel skeletons for powerful cnn via asymmetric convolution blocks. In *Proceedings of the IEEE/CVF international conference on computer vision*, pages 1911–1920, 2019. [5](#), [14](#)
- [7] Xiaohan Ding, Tianxiang Hao, Jianchao Tan, Ji Liu, Jungong Han, Yuchen Guo, and Guiguang Ding. Lossless cnn channel pruning via decoupling remembering and forgetting. In *ICCV*, 2021. [3](#)
- [8] Xiaohan Ding, Chunlong Xia, Xiangyu Zhang, Xiaojie Chu, Jungong Han, and Guiguang Ding. Repmlp: Re-parameterizing convolutions into fully-connected layers for image recognition. *arXiv preprint arXiv:2105.01883*, 2021. [3](#)
- [9] Xiaohan Ding, Xiangyu Zhang, Jungong Han, and Guiguang Ding. Diverse branch block: Building a convolution as an inception-like unit. In *Proceedings of the IEEE/CVF Conference on Computer Vision and Pattern Recognition*, pages 10886–10895, 2021. [1](#), [3](#)
- [10] Xiaohan Ding, Xiangyu Zhang, Ningning Ma, Jungong Han, Guiguang Ding, and Jian Sun. Repvgg: Making vgg-style convnets great again. In *Proceedings of the IEEE/CVF conference on computer vision and pattern recognition*, pages 13733–13742, 2021. [1](#), [3](#), [4](#), [5](#), [14](#)
- [11] Alexey Dosovitskiy, Lucas Beyer, Alexander Kolesnikov, Dirk Weissenborn, Xiaohua Zhai, Thomas Unterthiner, Mostafa Dehghani, Matthias Minderer, Georg Heigold, Sylvain Gelly, et al. An image is worth 16x16 words: Transformers for image recognition at scale. *arXiv preprint arXiv:2010.11929*, 2020. [3](#), [4](#)
- [12] Jun Fu, Jing Liu, Haijie Tian, Yong Li, Yongjun Bao, Zhiwei Fang, and Hanqing Lu. Dual attention network for scene segmentation. In *IEEE Conf. Comput. Vis. Pattern Recog.*, pages 3146–3154, 2019. [3](#)
- [13] Si Gao, Chengjian Zheng, Xiaofeng Zhang, Shaoli Liu, Biao Wu, Kaidi Lu, Diankai Zhang, and Ning Wang. Rcbsr: re-parameterization convolution block for super-resolution. In *Computer Vision–ECCV 2022 Workshops: Tel Aviv, Israel, October 23–27, 2022, Proceedings, Part II*, pages 540–548. Springer, 2023. [3](#)
- [14] Xifeng Gao, Zhigang Deng, and Guoning Chen. Hexahedral mesh re-parameterization from aligned base-complex. *ACM Transactions on Graphics (TOG)*, 34(4):1–10, 2015. [3](#)
- [15] Zilin Gao, Jiangtao Xie, Qilong Wang, and Peihua Li. Global second-order pooling convolutional networks. In *IEEE Conf. Comput. Vis. Pattern Recog.*, pages 3024–3033, 2019. [3](#)
- [16] Jingda Guo, Xu Ma, Andrew Sansom, Mara McGuire, Andrew Kalaani, Qi Chen, Sihai Tang, Qing Yang, and Song Fu. Spanet: Spatial pyramid attention network for enhanced image recognition. In *2020 IEEE International Conference on Multimedia and Expo (ICME)*, pages 1–6. IEEE, 2020. [3](#), [5](#), [6](#)
- [17] Shuxuan Guo, Jose M. Alvarez, and Mathieu Salzmann. Expandnets: linear over re-parameterization to train compact convolutional networks. In *NeurIPS*, 2020. [1](#), [3](#)
- [18] Kaiming He, Xiangyu Zhang, Shaoqing Ren, and Jian Sun. Deep residual learning for image recognition. In *IEEE Conf. Comput. Vis. Pattern Recog.*, pages 770–778, 2016. [2](#), [4](#), [14](#)
- [19] Qibin Hou, Daquan Zhou, and Jiashi Feng. Coordinate attention for efficient mobile network design. *arXiv preprint arXiv:2103.02907*, 2021. [3](#)
- [20] Andrew G Howard, Menglong Zhu, Bo Chen, Dmitry Kalenichenko, Weijun Wang, Tobias Weyand, Marco Andreetto, and Hartwig Adam. Mobilenets: Efficient convolutional neural networks for mobile vision applications. *arXiv preprint arXiv:1704.04861*, 2017. [4](#), [14](#)
- [21] Jie Hu, Li Shen, Samuel Albanie, Gang Sun, and Andrea Vedaldi. Gather-excite: Exploiting feature context in convolutional neural networks. In *Adv. Neural Inform. Process. Syst.*, pages 9401–9411, 2018. [3](#)
- [22] Jie Hu, Li Shen, and Gang Sun. Squeeze-and-excitation networks. In *IEEE Conf. Comput. Vis. Pattern Recog.*, pages 7132–7141, 2018. [2](#), [3](#), [5](#), [6](#), [7](#)
- [23] Mu Hu, Junyi Feng, Jiashen Hua, Baisheng Lai, Jianqiang Huang, Xiaojin Gong, and Xian-Sheng Hua. Online convolutional re-parameterization. In *Proceedings of the IEEE/CVF Conference on Computer Vision and Pattern Recognition*, pages 568–577, 2022. [1](#), [3](#)
- [24] Tao Huang, Shan You, Bohan Zhang, Yuxuan Du, Fei Wang, Chen Qian, and Chang Xu. Dyrep: Bootstrapping training with dynamic re-parameterization. In *Proceedings of*

- the *IEEE/CVF Conference on Computer Vision and Pattern Recognition*, pages 588–597, 2022. 3
- [25] Zhongzhan Huang, Mingfu Liang, and Liang Lin. On robust numerical solver for ode via self-attention mechanism. *arXiv preprint arXiv:2302.10184*, 2023. 12
- [26] Zhongzhan Huang, Senwei Liang, Mingfu Liang, Weiling He, and Liang Lin. Layer-wise shared attention network on dynamical system perspective. *arXiv preprint arXiv:2210.16101*, 2022. 3
- [27] Zhongzhan Huang, Senwei Liang, Mingfu Liang, Wei He, Haizhao Yang, and Liang Lin. The lottery ticket hypothesis for self-attention in convolutional neural network. *arXiv preprint arXiv:2207.07858*, 2022. 6
- [28] Zhongzhan Huang, Senwei Liang, Mingfu Liang, and Haizhao Yang. Dianet: Dense-and-implicit attention network. In *AAAI*, pages 4206–4214, 2020. 3
- [29] Sergey Ioffe and Christian Szegedy. Batch normalization: Accelerating deep network training by reducing internal covariate shift. In *International conference on machine learning*, pages 448–456. pmlr, 2015. 13
- [30] Takeshi Kojima, Yutaka Matsuo, and Yusuke Iwasawa. Robustifying vision transformer without retraining from scratch by test-time class-conditional feature alignment. *arXiv preprint arXiv:2206.13951*, 2022. 5
- [31] Alex Krizhevsky, Geoffrey Hinton, et al. Learning multiple layers of features from tiny images. 2009. 5
- [32] HyunJae Lee, Hyo-Eun Kim, and Hyeonseob Nam. Srm: A style-based recalibration module for convolutional neural networks. In *Int. Conf. Comput. Vis.*, pages 1854–1862, 2019. 3, 5, 7
- [33] Xiang Li, Xiaolin Hu, and Jian Yang. Spatial group-wise enhance: Improving semantic feature learning in convolutional networks. *arXiv preprint arXiv:1905.09646*, 2019. 3
- [34] Xiang Li, Wenhai Wang, Xiaolin Hu, and Jian Yang. Selective kernel networks. In *IEEE Conf. Comput. Vis. Pattern Recog.*, pages 510–519, 2019. 3
- [35] Senwei Liang, Zhongzhan Huang, Mingfu Liang, and Haizhao Yang. Instance enhancement batch normalization: An adaptive regulator of batch noise. In *Proceedings of the AAAI Conference on Artificial Intelligence*, volume 34, pages 4819–4827, 2020. 3, 5, 6, 7, 16
- [36] Tsung-Yi Lin, Michael Maire, Serge Belongie, James Hays, Pietro Perona, Deva Ramanan, Piotr Dollár, and C Lawrence Zitnick. Microsoft coco: Common objects in context. In *Eur. Conf. Comput. Vis.*, pages 740–755, 2014. 5
- [37] Jiaji Luo, Weijian Si, and Zhian Deng. Few-shot learning for radar signal recognition based on tensor imprint and re-parameterization multi-channel multi-branch model. *IEEE Signal Processing Letters*, 29:1327–1331, 2022. 3
- [38] Tian Lv, Chongyang Bai, and Chaojie Wang. Mdmmlp: Image classification from scratch on small datasets with mlp. *arXiv preprint arXiv:2205.14477*, 2022. 5
- [39] Ningning Ma, Xiangyu Zhang, Hai-Tao Zheng, and Jian Sun. Shufflenet v2: Practical guidelines for efficient cnn architecture design. In *Proceedings of the European conference on computer vision (ECCV)*, pages 116–131, 2018. 4, 14
- [40] Igor Ogashawara, Deepak R Mishra, Renata FF Nascimento, Enner H Alcântara, Milton Kampel, and Jose L Stech. Re-parameterization of a quasi-analytical algorithm for colored dissolved organic matter dominant inland waters. *International Journal of Applied Earth Observation and Geoinformation*, 53:128–145, 2016. 3
- [41] Jongchan Park, Sanghyun Woo, Joon-Young Lee, and In So Kweon. Bam: Bottleneck attention module. *arXiv preprint arXiv:1807.06514*, 2018. 3
- [42] Zequn Qin, Pengyi Zhang, Fei Wu, and Xi Li. Fcanet: Frequency channel attention networks. In *Proceedings of the IEEE/CVF international conference on computer vision*, pages 783–792, 2021. 3
- [43] Abhijit Guha Roy, Nassir Navab, and Christian Wachinger. Recalibrating fully convolutional networks with spatial and channel “squeeze and excitation” blocks. *IEEE Medical Imaging*, pages 540–549, 2018. 3
- [44] Olga Russakovsky, Jia Deng, Hao Su, Jonathan Krause, Sanjeev Satheesh, Sean Ma, Zhiheng Huang, Andrej Karpathy, Aditya Khosla, Michael Bernstein, et al. Imagenet large scale visual recognition challenge. *International journal of computer vision*, 115(3):211–252, 2015. 2, 5
- [45] Benjamín J Sánchez, José R Pérez-Correa, and Eduardo Agosin. Construction of robust dynamic genome-scale metabolic model structures of *saccharomyces cerevisiae* through iterative re-parameterization. *Metabolic engineering*, 25:159–173, 2014. 3
- [46] Ramprasaath R. Selvaraju, Michael Cogswell, Abhishek Das, Ramakrishna Vedantam, Devi Parikh, and Dhruv Batra. Grad-cam: Visual explanations from deep networks via gradient-based localization. In *International Conference on Computer Vision*, 2017. 7
- [47] Karen Simonyan and Andrew Zisserman. Very deep convolutional networks for large-scale image recognition. *arXiv preprint arXiv:1409.1556*, 2014. 4, 14
- [48] Kartik Surisetty, Hector De la Hoz Siegler, William C McCaffrey, and Amos Ben-Zvi. Model re-parameterization and output prediction for a bioreactor system. *Chemical engineering science*, 65(16):4535–4547, 2010. 3
- [49] Hugo Touvron, Piotr Bojanowski, Mathilde Caron, Matthieu Cord, Alaaeldin El-Nouby, Edouard Grave, Gautier Izacard, Armand Joulin, Gabriel Synnaeve, Jakob Verbeek, et al. Resmlp: Feedforward networks for image classification with data-efficient training. *IEEE Transactions on Pattern Analysis and Machine Intelligence*, 2022. 3
- [50] Hugo Touvron, Matthieu Cord, Matthijs Douze, Francisco Massa, Alexandre Sablayrolles, and Hervé Jégou. Training data-efficient image transformers & distillation through attention. In *International conference on machine learning*, pages 10347–10357. PMLR, 2021. 3
- [51] Dmitry Ulyanov, Andrea Vedaldi, and Victor Lempitsky. Instance normalization: The missing ingredient for fast stylization. *arXiv preprint arXiv:1607.08022*, 2016. 13
- [52] Ashish Vaswani, Noam Shazeer, Niki Parmar, Jakob Uszkoreit, Llion Jones, Aidan N Gomez, Łukasz Kaiser, and Illia Polosukhin. Attention is all you need. In *Adv. Neural Inform. Process. Syst.*, pages 5998–6008, 2017. 3

- [53] Fei Wang, Mengqing Jiang, Chen Qian, Shuo Yang, Cheng Li, Honggang Zhang, Xiaogang Wang, and Xiaoou Tang. Residual attention network for image classification. In *IEEE Conf. Comput. Vis. Pattern Recog.*, pages 3156–3164, 2017. 3
- [54] Jiayun Wang, Yubei Chen, Stella X Yu, Brian Cheung, and Yann LeCun. Recurrent parameter generators. *arXiv preprint arXiv:2107.07110*, 2021. 5
- [55] Qilong Wang, Banggu Wu, Pengfei Zhu, Peihua Li, Wangmeng Zuo, and Qinghua Hu. Eca-net: Efficient channel attention for deep convolutional neural networks. In *IEEE Conf. Comput. Vis. Pattern Recog.*, pages 11534–11542, 2020. 3, 5
- [56] Xintao Wang, Chao Dong, and Ying Shan. Repsr: Training efficient vgg-style super-resolution networks with structural re-parameterization and batch normalization. In *Proceedings of the 30th ACM International Conference on Multimedia*, pages 2556–2564, 2022. 1, 3
- [57] Xiaolong Wang, Ross Girshick, Abhinav Gupta, and Kaiming He. Non-local neural networks. In *IEEE Conf. Comput. Vis. Pattern Recog.*, pages 7794–7803, 2018. 3
- [58] Sanghyun Woo, Jongchan Park, Joon-Young Lee, and In So Kweon. Cbam: Convolutional block attention module. In *Eur. Conf. Comput. Vis.*, pages 3–19, 2018. 3, 5
- [59] Yuxin Wu and Kaiming He. Group normalization. In *Proceedings of the European conference on computer vision (ECCV)*, pages 3–19, 2018. 13
- [60] Yibo Yang, Jianlong Wu, Hongyang Li, Xia Li, Tiancheng Shen, and Zhouchen Lin. Dynamical system inspired adaptive time stepping controller for residual network families. In *Proceedings of the AAAI Conference on Artificial Intelligence*, volume 34, pages 6648–6655, 2020. 12
- [61] Weihao Yu, Mi Luo, Pan Zhou, Chenyang Si, Yichen Zhou, Xinchao Wang, Jiashi Feng, and Shuicheng Yan. Metaformer is actually what you need for vision. In *Proceedings of the IEEE/CVF conference on computer vision and pattern recognition*, pages 10819–10829, 2022. 3
- [62] Li Yuan, Yunpeng Chen, Tao Wang, Weihao Yu, Yujun Shi, Zi-Hang Jiang, Francis EH Tay, Jiashi Feng, and Shuicheng Yan. Tokens-to-token vit: Training vision transformers from scratch on imagenet. In *Proceedings of the IEEE/CVF international conference on computer vision*, pages 558–567, 2021. 3
- [63] Hang Zhang, Chongruo Wu, Zhongyue Zhang, Yi Zhu, Zhi Zhang, Haibin Lin, Yue Sun, Tong He, Jonas Mueller, R Manmatha, et al. Resnest: Split-attention networks. *arXiv preprint arXiv:2004.08955*, 2020. 3
- [64] Mingyang Zhang, Xinyi Yu, Jingtao Rong, and Linlin Ou. Repnas: Searching for efficient re-parameterizing blocks. *arXiv 2109.03508*, 2021. 3
- [65] Ruiteng Zhang, Jianguo Wei, Wenhuan Lu, Lin Zhang, Yantao Ji, Junhai Xu, and Xugang Lu. Cs-rep: Making speaker verification networks embracing re-parameterization. In *ICASSP 2022-2022 IEEE International Conference on Acoustics, Speech and Signal Processing (ICASSP)*, pages 7082–7086. IEEE, 2022. 3
- [66] Shanshan Zhong, Wushao Wen, and Jinghui Qin. Mix-pooling strategy for attention mechanism. *arXiv preprint arXiv:2208.10322*, 2022. 3
- [67] Hengyi Zhou, Longjun Liu, Haonan Zhang, Hongyi He, and Nanning Zheng. Cmb: A novel structural re-parameterization block without extra training parameters. In *2022 International Joint Conference on Neural Networks (IJCNN)*, pages 1–9. IEEE, 2022. 3
- [68] Xizhou Zhu, Dazhi Cheng, Zheng Zhang, Stephen Lin, and Jifeng Dai. An empirical study of spatial attention mechanisms in deep networks. In *Int. Conf. Comput. Vis.*, pages 6688–6697, 2019. 3

A. The Proof of Theorem 6.1

Theorem 6.1 Consider ASR for a L layers residual neural network with self-attention module $T(\cdot)$, and the corresponding constant input at t -th layer ψ_t , i.e., $x_{t+1} = x_t + f(x_t; W_t) \odot T[f(\psi_t)]$, $t = 0, 1, \dots, L - 1$. Let ϵ be the perturbation from the noise and satisfies $\|x_0^\epsilon - x_0\| = \epsilon$, and $\epsilon_t = \|x_t^\epsilon - x_t\|$, we have

$$\epsilon_{t+1} \leq \epsilon_t (1 + \alpha_t \|W_t\|_2), \quad (10)$$

where $\alpha_t = \max\{T[f(\psi_t)]\}$ and \max refers to the largest element in a vector. See proof in the appendix.

Proof. Let $H(x) = f(x_t; W_t) \odot T[f(\psi_t)]$, according to Taylor expansion, we have

$$H(x_t^\epsilon) = H(x_t) + (x_t^\epsilon - x_t)^T \nabla_x H(x)|_{x=x_t} \quad (11)$$

For $\epsilon_{t+1} = \|x_{t+1}^\epsilon - x_{t+1}\|$, we have

$$\begin{aligned} \epsilon_{t+1} &= \|x_{t+1}^\epsilon - x_{t+1}\| \\ &= \|x_t^\epsilon + f(x_t^\epsilon; W_t) \odot T[f(\psi_t)] - x_t - f(x_t; W_t) \odot T[f(\psi_t)]\| \\ &= \|(x_t^\epsilon - x_t) + f(x_t^\epsilon; W_t) \odot T[f(\psi_t)] - f(x_t; W_t) \odot T[f(\psi_t)]\| \\ &= \|(x_t^\epsilon - x_t) + (x_t^\epsilon - x_t)^T \nabla_x H(x)|_{x=x_t}\| && \text{Since Eq.(11)} \\ &\leq \|(x_t^\epsilon - x_t)\| \cdot (1 + \|\nabla_x H(x)|_{x=x_t}\|) && \text{Since } \|ab\| \leq \|a\| \|b\| \\ &= \epsilon_t (1 + \|\nabla_x H(x)|_{x=x_t}\|) \end{aligned}$$

Next, we analyze $\nabla_x H(x)|_{x=x_t}$. We also follow and consider the assumption [60, 25] that $f(x_t; W_t)$ is consists of linear transformation and ReLU non-linear activation \mathbf{A} , i.e., $f(x_t; W_t) = \mathbf{A}W_t x_t$. Note that \mathbf{A} is a diagonal matrix

$$\mathbf{A} = \text{diag}(a_1, a_2, \dots, a_d), \quad a_1, a_2, \dots, a_d \in \{0, 1\}, \quad (12)$$

where d is dimension of x_t and each element $a_i, i = 1, 2, \dots, d$ in \mathbf{A} is 0 or 1. If the i^{th} element in x_t is positive, the value of $a_i = 1$, otherwise equals to zero. Therefore the 2-norm, i.e., the largest singular value, of \mathbf{A} is less than 1, i.e.,

$$\|\mathbf{A}\|_2 = \sqrt{\lambda_{\max} \mathbf{A}^T \mathbf{A}} = \sqrt{\lambda_{\max} \mathbf{A}} \leq 1 \quad (13)$$

Hence, we can further estimate $\|\nabla_x H(x)|_{x=x_t}\|$ that

$$\begin{aligned} \|\nabla_x H(x)|_{x=x_t}\| &= \|\nabla_x f(x; W_t)|_{x=x_t} \odot T[f(\psi_t)] + f(x_t; W_t) \odot \nabla_x T[f(\psi_t)]\| \\ &\leq \|\mathbf{A}W_t \mathbf{I} \odot T[f(\psi_t)]\| + 0 \\ &\leq \alpha_t \cdot \|\mathbf{A}\| \|W_t\| \\ &\leq \alpha_t \|W_t\| && \text{Since Eq.(13)} \end{aligned}$$

Therefore, we have $\epsilon_{t+1} \leq \epsilon_t (1 + \alpha_t \|W_t\|_2)$.

□

B. ASR for different neural network layers in inference phase

In the main text, we find that the “attention values” $\mathbf{v}_{\psi,\theta}$ generated by ASR are some constant vector, for the various common-used modules $\mathbf{B}_{\hat{\theta}}$ in the backbone, we can seamlessly find the corresponding transformation g such that

$$\mathbf{B}_{\hat{\theta}} \odot \mathbf{v}_{\psi,\theta} = \mathbf{B}_{g[\hat{\theta},\psi,\theta]}, \quad (14)$$

(1) For the convolutional layer, if $\mathbf{B}_{\hat{\theta}}$ is a convolutional layer \mathcal{C} with kernels \mathbf{K} and bias \mathbf{b} , then we have

$$\begin{aligned} \mathcal{C}(\mathbf{x}; \mathbf{K}, \mathbf{b}) \odot \mathbf{v}_{\psi,\theta} &= (\mathbf{x} * \mathbf{K}) \odot \mathbf{v}_{\psi,\theta} + \mathbf{b} \odot \mathbf{v}_{\psi,\theta} \\ &= \mathbf{x} * (\mathbf{K} \odot \mathbf{v}_{\psi,\theta}) + \mathbf{b} \odot \mathbf{v}_{\psi,\theta} \\ &= \mathcal{C}(\mathbf{x}; \mathbf{K} \odot \mathbf{v}_{\psi,\theta}, \mathbf{b} \odot \mathbf{v}_{\psi,\theta}), \\ &\equiv \mathcal{C}(\mathbf{x}; \mathbf{K}', \mathbf{b}') \end{aligned} \quad (15)$$

where $*$ denote convolution and $\mathbf{K} \odot \mathbf{v}_{\psi,\theta}$ means that the the product of i -th elements of $\mathbf{v}_{\psi,\theta}$ and i -th kernel of \mathbf{K} . Since the existing SRP methods mainly merge various neural network layers into a convolutional layer, therefore ASR is compatible with most of these SRP methods.

(2) For the normalization layer κ , like batch normalization [51], instance normalization [29], group normalization [59], etc., they generally can be formulated as

$$\kappa(x; \mu, \sigma, \gamma, \beta) = \frac{x - \mu}{\sigma} \odot \gamma + \beta, \quad (16)$$

where $\mu, \sigma, \gamma, \beta$ are the parameters of each kind of normalization method. For ASR, the Eq.(14) can be rewritten as

$$\begin{aligned} \kappa(\mathbf{x}; \mu, \sigma, \gamma, \beta) \odot \mathbf{v}_{\psi,\theta} &= \frac{(\mathbf{x} - \mu) \odot \gamma \odot \mathbf{v}_{\psi,\theta}}{\sigma} + \beta \odot \mathbf{v}_{\psi,\theta} \\ &= \kappa(\mathbf{x}; \gamma \odot \mathbf{v}_{\psi,\theta}, \beta \odot \mathbf{v}_{\psi,\theta}), \\ &\equiv \kappa(\mathbf{x}; \mu, \sigma, \gamma', \beta') \end{aligned} \quad (17)$$

(3) For the fully connected layer $f(x) = Wx$, we have

$$\begin{aligned} f(x) \odot \mathbf{v}_{\psi,\theta} &= Wx \odot \mathbf{v}_{\psi,\theta} \\ &= (W \odot \mathbf{v}_{\psi,\theta})x \equiv W'x \end{aligned} \quad (18)$$

(4) For the transformer-based attention layer T , we have

$$\begin{aligned} T(x; W_Q, W_K, W_V) \odot \mathbf{v}_{\psi,\theta} &= \frac{W_Q x (W_K x)^T}{\sqrt{d_k}} W_V x \odot \mathbf{v}_{\psi,\theta} \\ &= \frac{W_Q x (W_K x)^T}{\sqrt{d_k}} (W_V \odot \mathbf{v}_{\psi,\theta}) x \\ &\equiv \frac{W_Q x (W_K x)^T}{\sqrt{d_k}} W'_V x \\ &= T(x; W_Q, W_K, W'_V) \end{aligned} \quad \text{Since Eq.(18)}$$

C. Introduction of implementation details

In Section C.1, we present the experimental details, followed by an explanation in Section C.2 on how ASR is incorporated into various backbones.

C.1. Experiment details

Unless otherwise specified, we follow the settings of [18, 47, 10, 39, 20, 6]. Specifically, all models are trained on Nvidia RTX 3080 GPUs using STL10, CIFAR10, and CIFAR100 datasets, with epoch set to 164. For ImageNet, we train the models on eight Nvidia RTX 3080 GPUs and set the epoch to 100. During training, we apply standard data augmentation techniques such as normalization, random cropping, and horizontal flipping. The batch size of CIFAR10, CIFAR100, STL10 and ImageNet is 128, 128, 16, and 128 respectively. The other hyper-parameter settings of CIFAR10, CIFAR100, STL10 and ImageNet are shown in Table 10 and Table 11 respectively.

	ResNet83	ResNet164	VGG19	ShuffleNetV2	MobileNet	ViT	RepVGG	ResNet-ACNet
optimizer	SGD (0.9)	SGD (0.9)	SGD (0.9)	SGD (0.9)	SGD (0.9)	SGD (0.9)	SGD (0.9)	SGD (0.9)
schedule	81/122	81/122	60/120/160	60/120/160	60/120/160	cosine annealing	130	cosine annealing
weight decay	1.00E-04	1.00E-04	5.00E-04	5.00E-04	5.00E-04	5.00E-05	1.00E-04	1.00E-04
gamma	0.1	0.1	0.2	0.2	0.2	0.1	0.1	0.333
lr	0.1	0.1	0.1	0.1	0.1	0.1	0.1	0.1

Table 10. Implementation details for **CIFAR10/100, STL10** image classification. Normalization and standard data augmentation (random cropping and horizontal flipping) are applied to the training data.

	ResNet18	ResNet35	ResNet50
optimizer	SGD (0.9)	SGD (0.9)	SGD (0.9)
schedule	30/60/90	30/60/90	30/60/90
weight decay	1.00E-04	1.00E-04	1.00E-04
gamma	0.1	0.1	0.1
lr	0.1	0.1	0.1

Table 11. Implementation details for **ImageNet 2012** image classification. Normalization and standard data augmentation (random cropping and horizontal flipping) are applied to the training data. The random cropping of size 224 by 224 is used in these experiments.

Name	Explanation
optimizer	Optimizer
depth	The depth of the network
schedule	Decrease learning rate at these epochs
wd	Weight decay
gamma	The multiplicative factor of learning rate decay
lr	Initial learning rate

Table 12. The additional explanation.

C.2. Application details

In this section, we provide detailed information on how we apply ASR to different architectures during the training phase. We focus on ResNet and ResNet-ACNet, VGG and RepVGG, ShuffleNetV2, MobileNet, and ViT. For each architecture, we specify the location of ASR within the block and provide a visualization to facilitate understanding.

ResNet and ResNet-ACNet are popular convolutional neural network architectures that use basic blocks or bottlenecks. In our experiments, we insert ASR after the last batch normalization layer and before the residual addition operation, as shown in Fig. 7.

VGG and RepVGG are two VGG-type convolutional neural network architectures that are widely used in computer vision applications. In our experiments, we insert ASR between the batch normalization layer and ReLU activation function, as

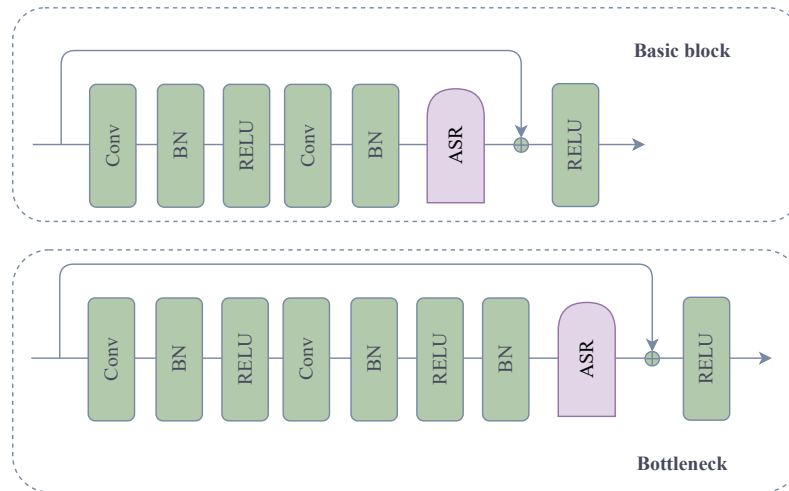


Figure 7. ASR in the blocks of ResNet during the training phase.

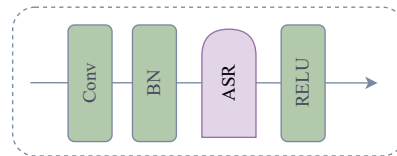


Figure 8. ASR in the block of VGG during the training phase.

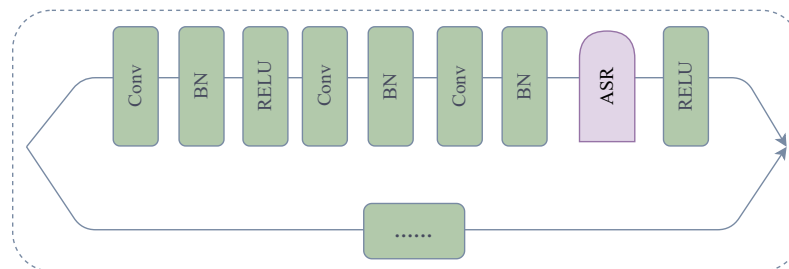


Figure 9. ASR in the block of ShuffleNetV2 during the training phase.

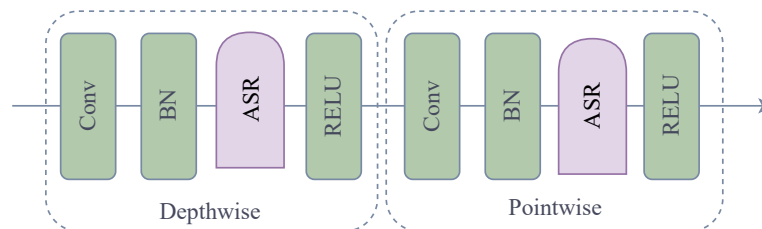


Figure 10. ASR in the block of MobileNet during the training phase.

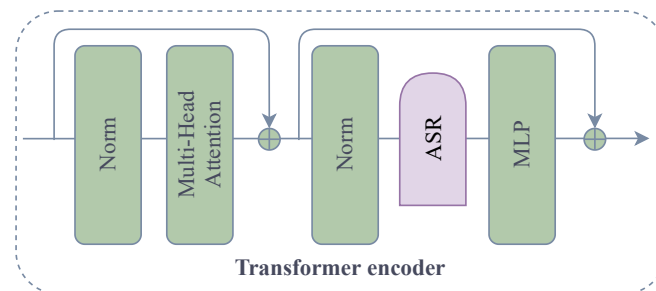


Figure 11. ASR in the transformer encoder of ViT during the training phase.

shown in Fig. 8. This location allows ASR to process the feature maps before they are passed to the next convolutional layer, which helps to reduce the batch noise [35] and distortion caused by the convolution.

ShuffleNetV2 is a lightweight convolutional neural network architecture that uses a dual-branch structure for its block. In our experiments, we insert ASR between the last batch normalization layer and ReLU activation function in the residual branch, as shown in Fig. 9.

MobileNet is another lightweight convolutional neural network architecture that uses depthwise and pointwise convolutional layers in each block. In our experiments, we insert ASR between BN and ReLU in both layers, as demonstrated in Fig. 10. This placement allows ASR to capture the non-linearity of both convolutional layers.

ViT. For ViT, we apply ASR to the transformer encoder, as illustrated in Fig. 11. ASR is inserted after Norm and before MLP. This placement allows ASR to avoid any interference with the multi-head attention mechanism.

D. The initialization of ASR

In this section, we analyze the initialization of the input $\psi \in R^{C \times 1 \times 1}$ in ASR. We conduct experiments by initializing ψ with values ranging from 0.1 to 0.6 and evaluate the performance of ASR on the CIFAR100 dataset as shown in Table 13. Our findings suggest that an appropriate initialization value is crucial for the performance of ASR. Specifically, we find that ASR initialized with a value of 0.1 achieves the highest accuracy of 74.83% and 74.77% on the test set, while the accuracy of ASR with other initialization values varies from 74.03% to 74.73%. These results indicate that choosing an appropriate initialization value can significantly impact the performance of ASR, and initializing ASR with a value of 0.1 leads to the best performance on the CIFAR100 dataset.

Initialization	0.1	0.2	0.3	0.4	0.5	0.6
ASR (SE)	74.83	<u>74.56</u>	74.15	74.17	74.03	74.15
ASR (IE)	74.77	<u>74.55</u>	<u>74.73</u>	74.25	74.45	74.24

Table 13. Top-1 accuracy (%) of different initialization values on ASR’s performance. The backbone is ResNet83, and the dataset is CIFAR100. Bold and underline indicate the best results and the second best results, respectively.

E. Different numbers of ASR inserted at the same position

In this section, we provide additional experimental results on the impact of inserting different numbers of ASR at the same position in ResNet164 and ViT. Specifically, we evaluate the performance of ResNet164 and ViT models with 1, 2, 3, and 4 ASR modules inserted at the positions shown in Fig. 7 and Fig. 11, respectively. We report the top-1 and top-5 accuracy on the CIFAR100 validation set.

As shown in Table 14, for ResNet164, the performance generally improves as the number of ASR modules increases when $\delta < 3$. These results suggest that inserting multiple ASR modules at the same position in ResNet164 may further enhance the performance. For ViT, as shown in Table 14, we observe a different trend where the performance decrease with an increasing number of ASR modules. These results suggest that although ASR can benefit ViT models, multiple ASR modules can not further improve their performance. Overall, the results demonstrate the effectiveness of ASR and suggest that inserting multiple ASR modules at the same position can potentially lead to even better performance.

Module		$\delta = 1$		$\delta = 2$		$\delta = 3$		$\delta = 4$	
		Top-1 acc.	Top-5 acc.	Top-1 acc.	Top-5 acc.	Top-1 acc.	Top-5 acc.	Top-1 acc.	Top-5 acc.
ResNet164	ASR (SE)	75.36	93.53	75.87	93.99	75.72	94.15	75.22	93.56
	ASR (IE)	75.58	93.84	75.71	93.81	75.45	94.07	74.56	93.73
	ASR (SRM)	75.23	93.68	75.45	94.06	75.61	94.21	75.11	93.78
	ASR (SPA)	75.12	93.44	75.43	93.66	75.81	94.03	75.62	93.46
ViT	ASR (SE)	67.82	87.80	66.74	86.77	65.43	83.33	59.78	81.08
	ASR (IE)	67.45	87.23	65.08	84.14	58.84	81.80	59.35	81.31
	ASR (SRM)	68.12	87.80	66.15	84.83	58.76	80.46	59.28	81.80
	ASR (SPA)	68.41	87.92	65.34	83.00	59.85	78.70	59.15	80.50

Table 14. The accuracy (%) of ResNet164 and ViT with different numbers of ASR inserted at the same position on CIFAR100.

F. The visualizations of the first-order difference (absolute value) for attention value over epoch

To provide further evidence for the claim made in our paper that most of the attention values almost converge at the first learning rate decay (30 epochs), we present additional visualizations of the first-order difference (absolute value) in attention value over epoch for different structures, attention modules, datasets, and training settings (including learning rate and weight decay). Each figure includes four subplots that show the evolution of attention value for different images. The horizontal axis indicates the number of epochs, while the vertical axis represents the order of random channel ID. Unless otherwise specified, we adopt ResNet83-SE as our baseline, CIFAR100 as the default dataset, and schedule learning rate as the default learning rate, with weight decay set to $1e-4$.

Different backbones. Fig. 12 and Fig. 13 show the first-order difference (absolute value) in attention value over epoch for ResNet83 and ResNet164, respectively. Both backbones exhibit the same trend, indicating that most of the attention values almost converge at the first learning rate decay (30 epochs).

Different attention modules. Fig. 12 and Fig. 14 present the first-order difference (absolute value) in attention value over epoch for two attention modules SE and IE, respectively. Although IE has some cchannel that converge more slowly than others, most of the channel attention values almost converge at 30 epochs.

Different datasets. Fig. 12 and Fig. 15 compare the attention values of ResNet83-SE on CIFAR100 and STL10 during the training process. Although ResNet83-SE exhibits greater attention value fluctuations in the initial stages on the STL10, our results still align with the findings presented in our paper.

Different training setting. We also compare the first-order difference (absolute value) in attention value over epoch for ResNet83-SE under different training settings. Fig. 12 and Fig. 16 show the results of using schedule learning rate and cosine learning rate, respectively. Fig. 17, Fig. 18, and Fig. 19 correspond to weight decay values of $2e-4$, $3e-4$, and $4e-4$, respectively. In all cases, we obtain results consistent with our paper’s findings. We also observe that larger weight decay values lead to faster attention value convergence.

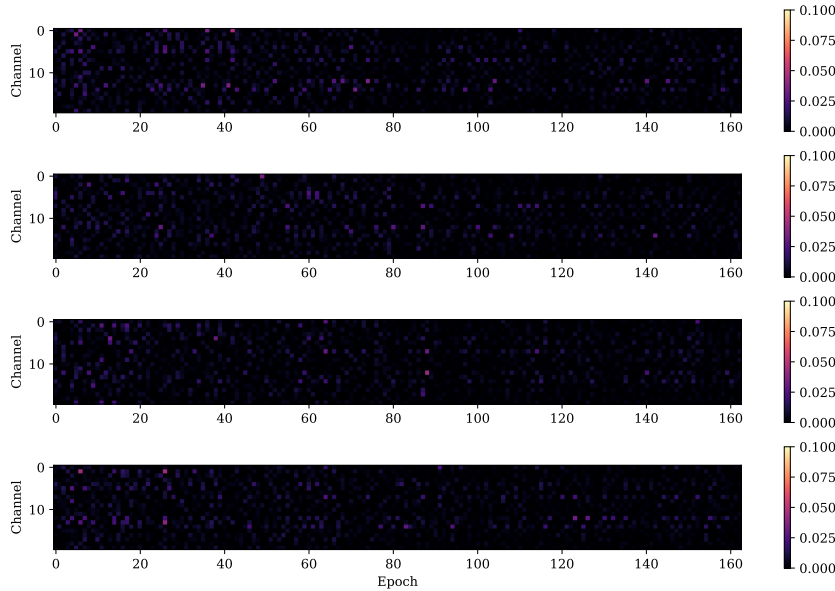


Figure 12. The visualization of the first-order difference (absolute value) for attention value of ResNet83-SE (weight decay: $1e-4$) over epoch on CIFAR100. Zoom in for best view.

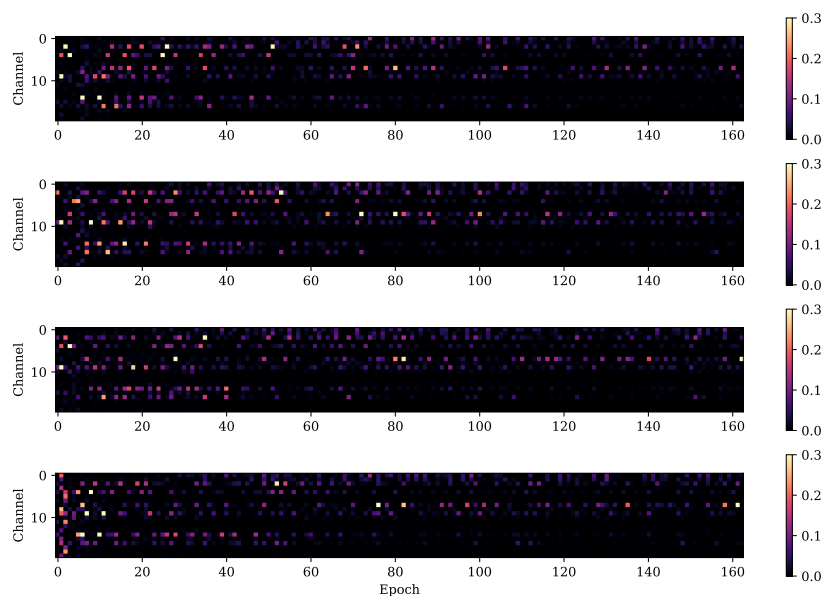


Figure 13. The visualization of the first-order difference (absolute value) for attention value of ResNet164-SE (weight decay: $1e-4$) over epoch on CIFAR100. Zoom in for best view.

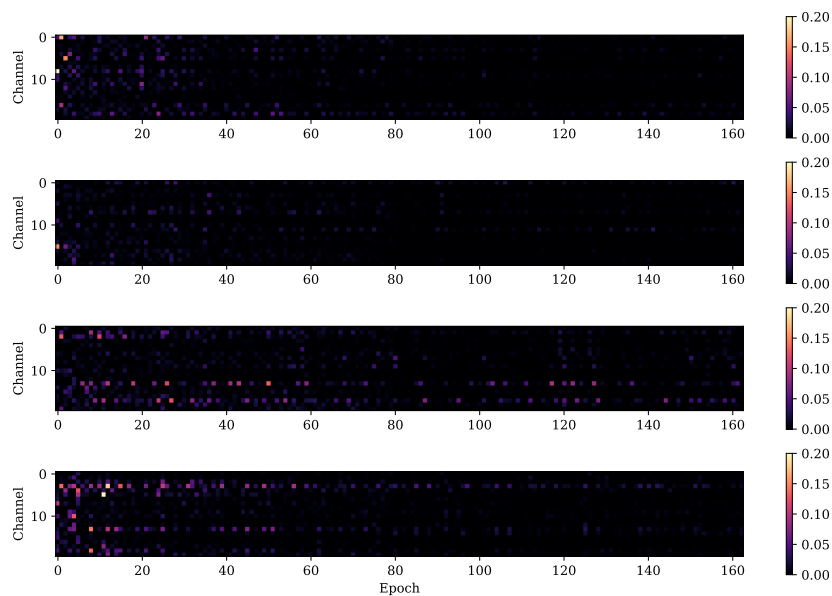


Figure 14. The visualization of the first-order difference (absolute value) for attention value of ResNet83-IE (weight decay: $1e-4$) over epoch on CIFAR100. Zoom in for best view.

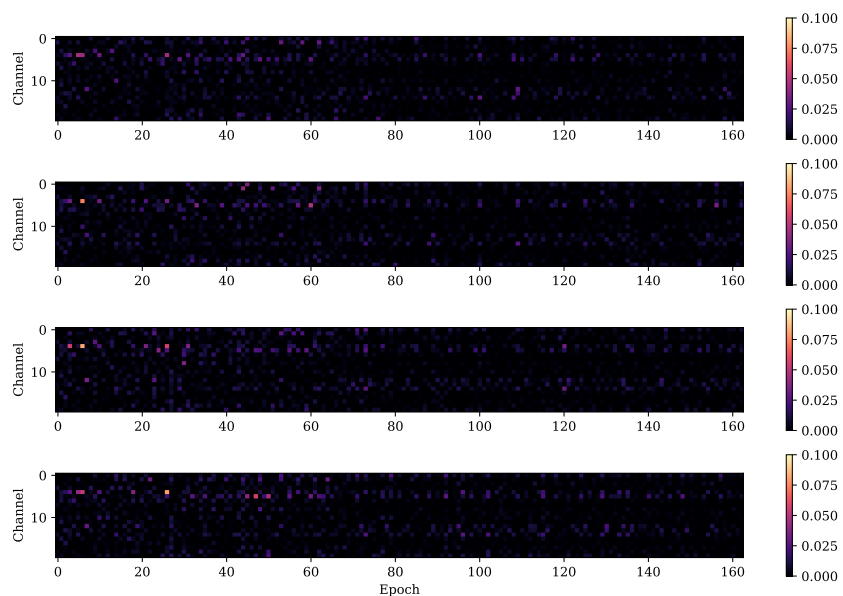


Figure 15. The visualization of the first-order difference (absolute value) for attention value of ResNet83-SE (weight decay: $1e-4$) over epoch on STL10. Zoom in for best view.

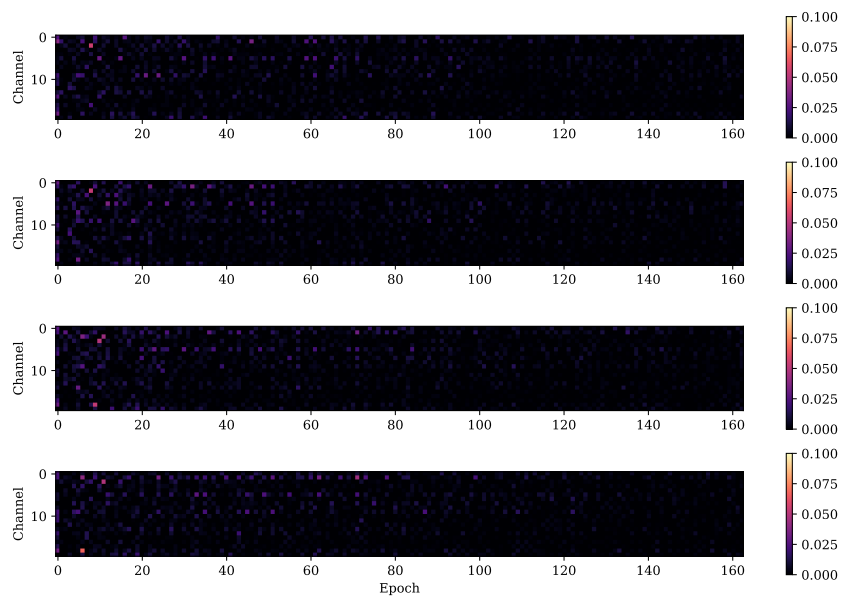


Figure 16. The visualization of the first-order difference (absolute value) for attention value of ResNet83-SE (weight decay: $1e-4$) based on cosine learning rate over epoch on CIFAR100. Zoom in for best view.

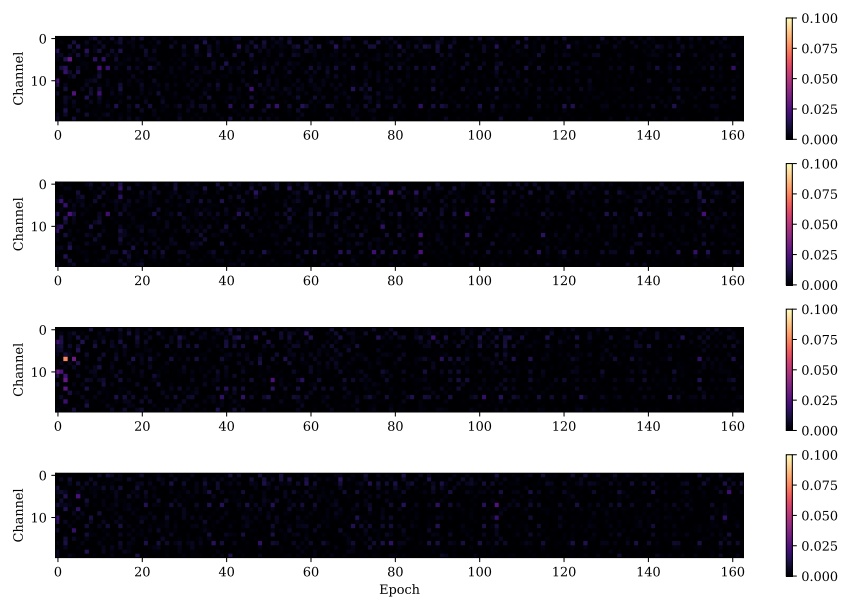


Figure 17. The visualization of the first-order difference (absolute value) for attention value of ResNet83-SE (weight decay: $2e-4$) over epoch on CIFAR100. Zoom in for best view.

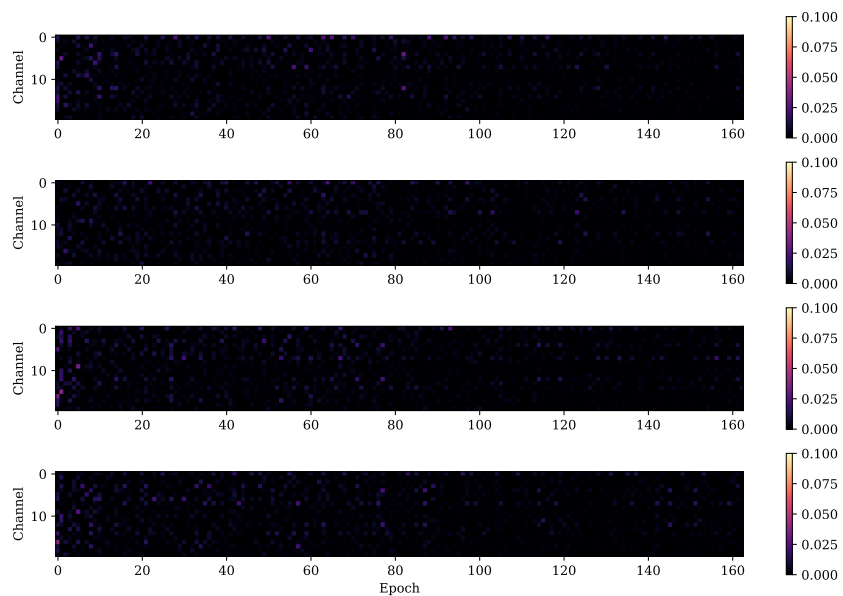


Figure 18. The visualization of the first-order difference (absolute value) for attention value of ResNet83-SE (weight decay: $3e-4$) over epoch on CIFAR100. Zoom in for best view.

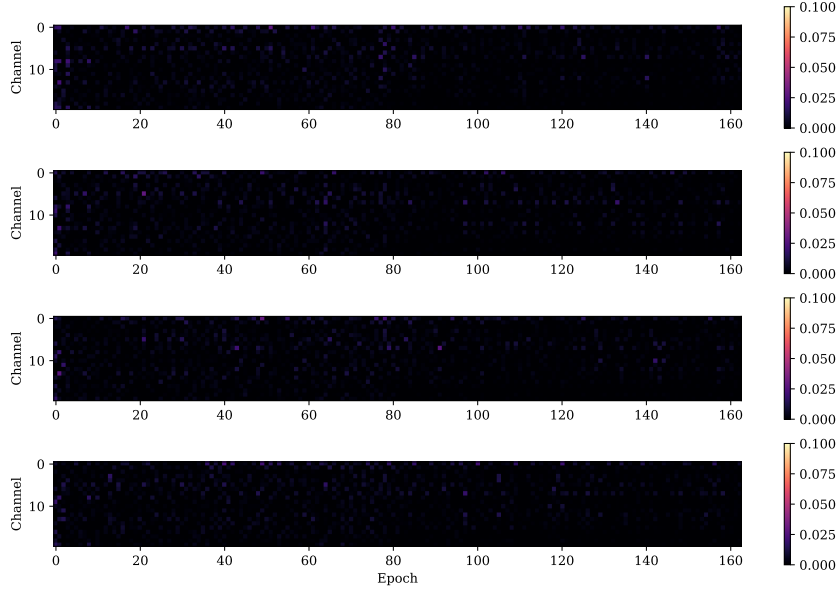


Figure 19. The visualization of the first-order difference (absolute value) for attention value of ResNet83-SE (weight decay: $4e-4$) over epoch on CIFAR100. Zoom in for best view.

G. The results about the batch noise attack

We conduct experiments on three types of noise attacks to empirically verify the ability of ASR in regulating noise to improve model robustness, including batch noise, constant noise, and random noise. We consider the style transfer task, which generally adopts the instance normalization (IN) without batch noise, rather than BN, as adding batch noise would significantly reduce the quality of generated images due to noise interference.

In this section, we present additional results on the batch noise attack to support the conclusions of our paper. As shown in Fig. 20, Fig. 21, and Fig. 22, with batch noise (BN), there are more blurriness compared to without batch noise (IN). However, when ASR is applied to BN, the aforementioned issues are significantly reduced. This suggests that ASR can effectively alleviate the adverse effects of noise introduced by batch normalization, resulting in image quality comparable to that of IN without batch noise.

H. The attention values of different images

In this section, we present additional examples to support the conclusions of our paper that after passing through the attention module, the channel attention values of different images tend to approach a certain value within the same channel, resulting in a “stripe structure”. We present in Fig. 23, Fig. 24, Fig. 25, Fig. 26, Fig. 27, Fig. 28, and Fig. 29 the visualization of attention values for different structures, attention modules, datasets, and training settings (including learning rate and weight decay values). The horizontal axis represents the order of random channels, while the vertical axis represents the order of random images. Corresponding to Appendix F, we use ResNet83-SE as the baseline, with the default dataset being CIFAR100, learning rate being schedule learning rate, and weight decay being $1e-4$. All figures show an obvious “stripe structure,” which is consistent with our conclusion in the paper that the attention values of different images tend to converge to a certain value within the same channel.

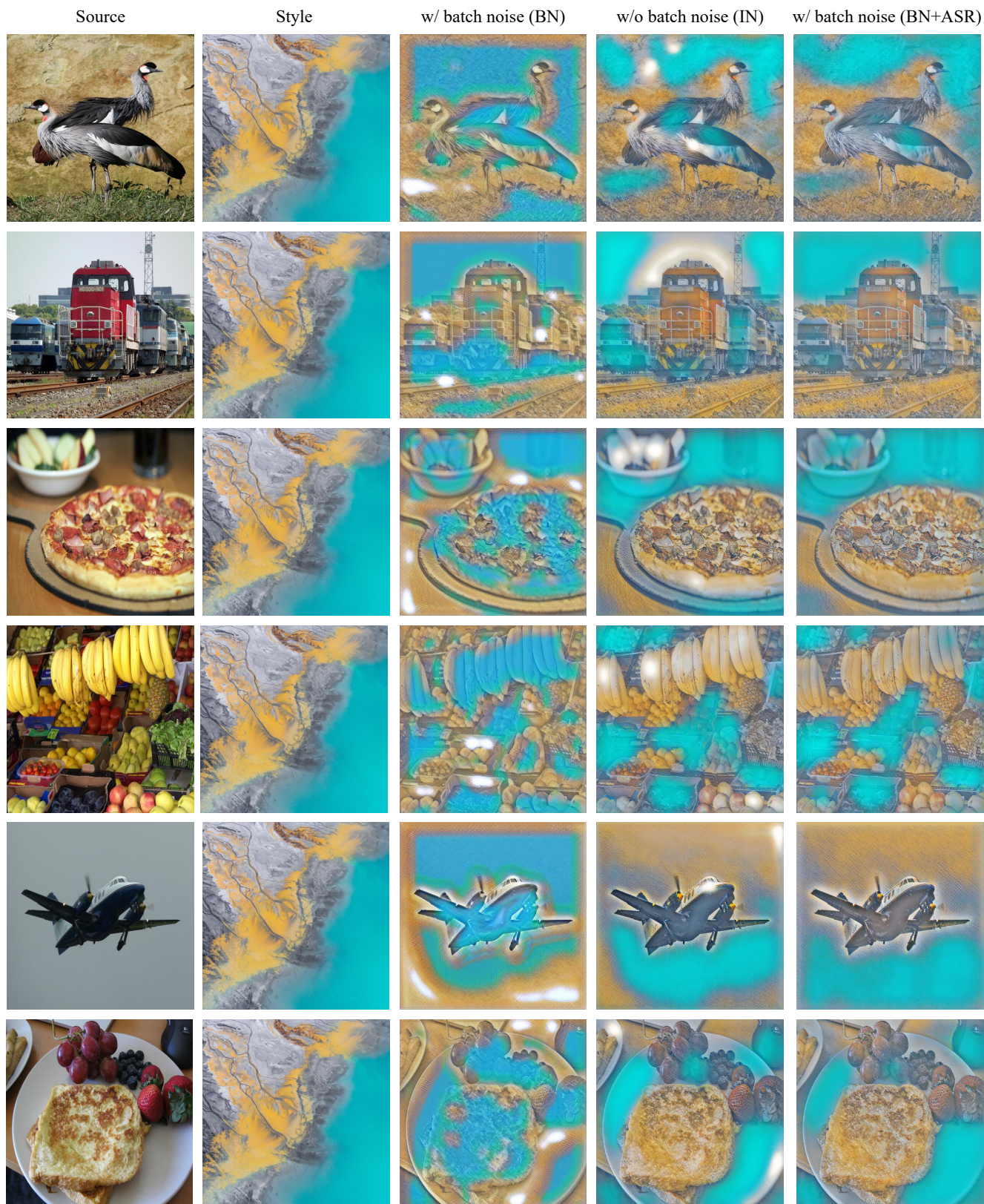


Figure 20. The results about the batch noise attack. Zoom in for best view.

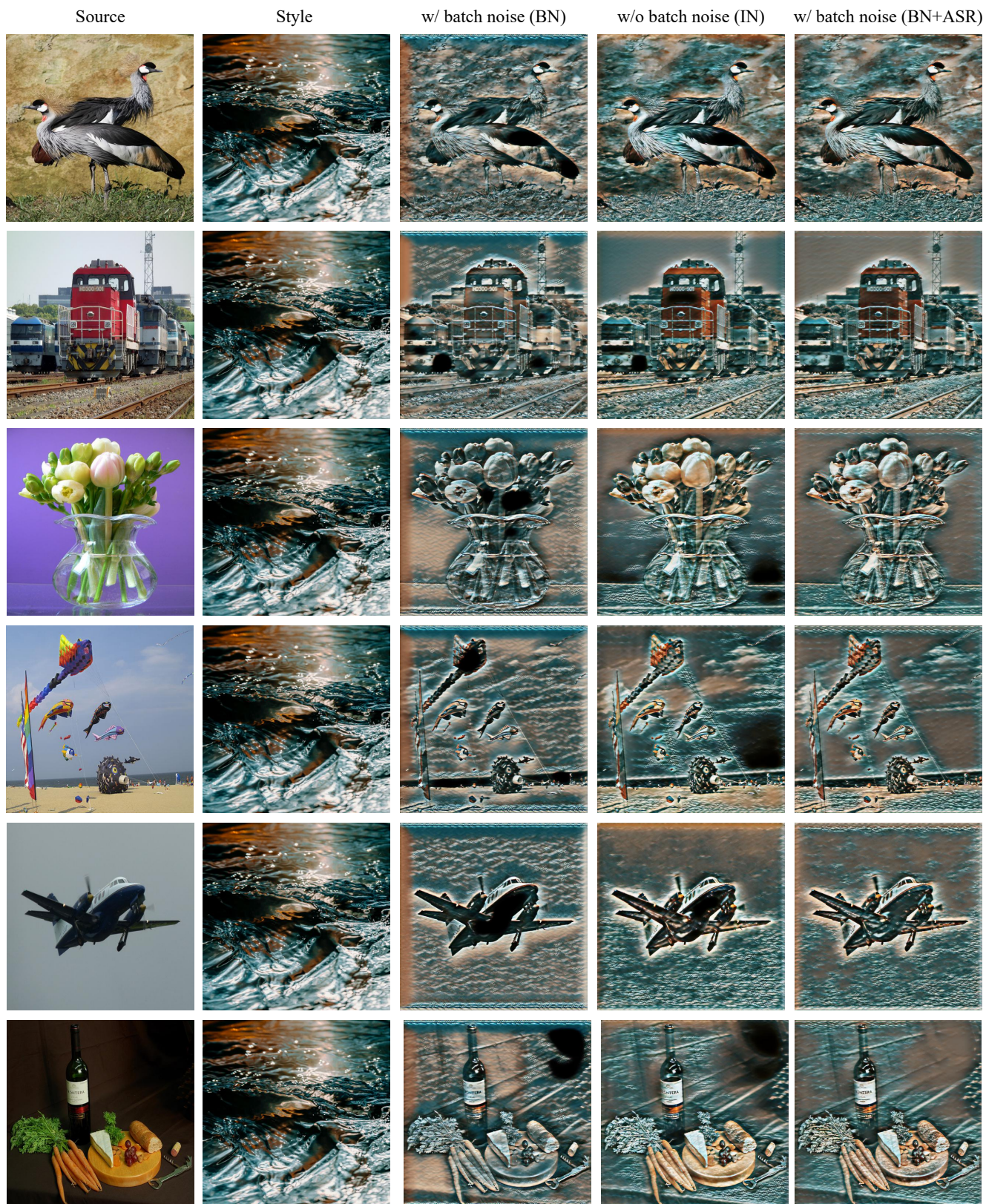


Figure 21. The results about the batch noise attack. Zoom in for best view.

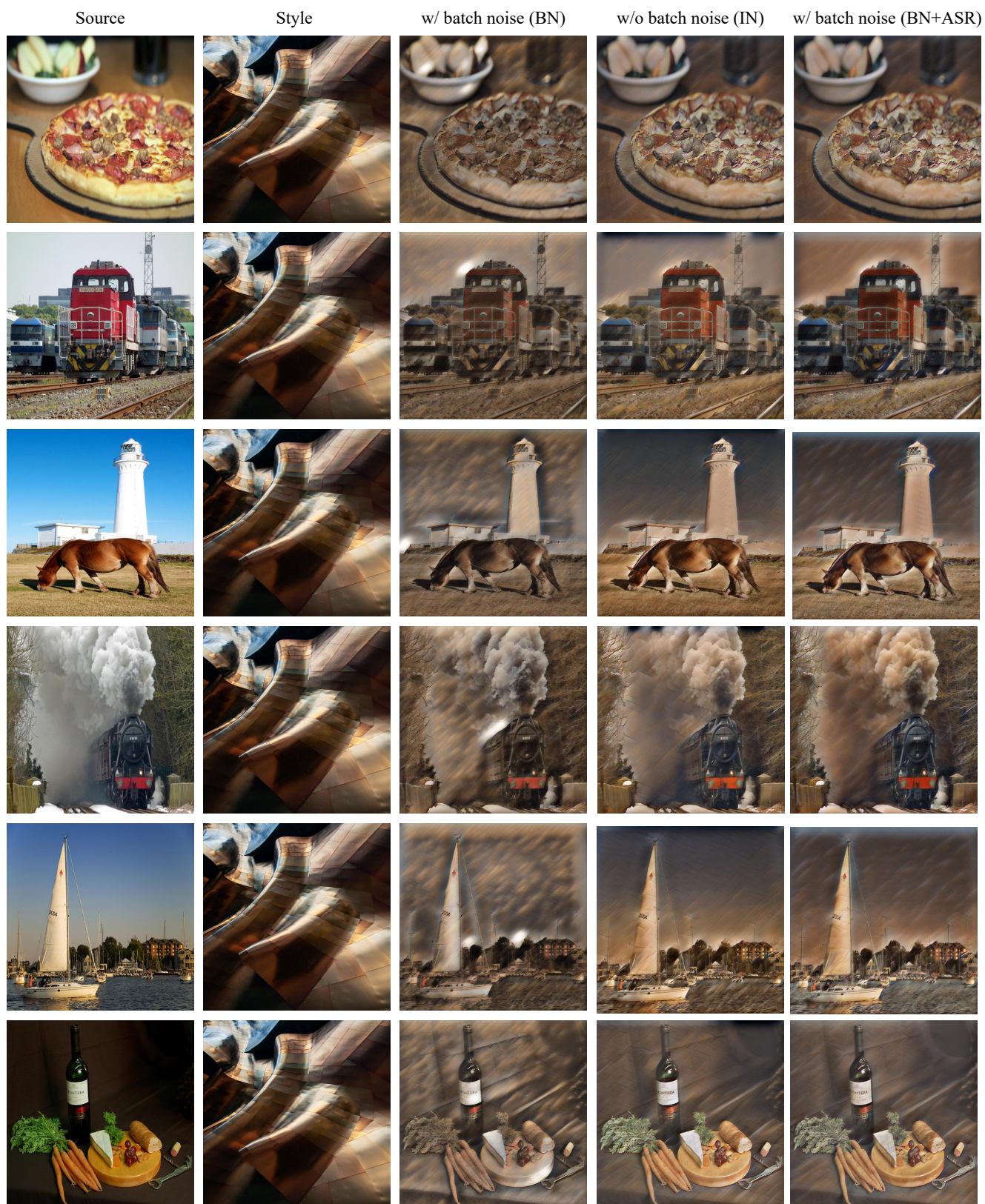


Figure 22. The results about the batch noise attack. Zoom in for best view.

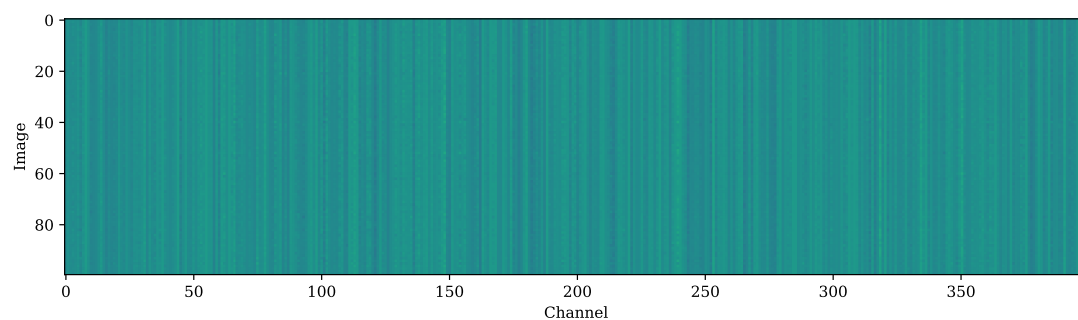


Figure 23. The attention values of different images from ResNet83-SE on CIFAR100. Zoom in for best view.

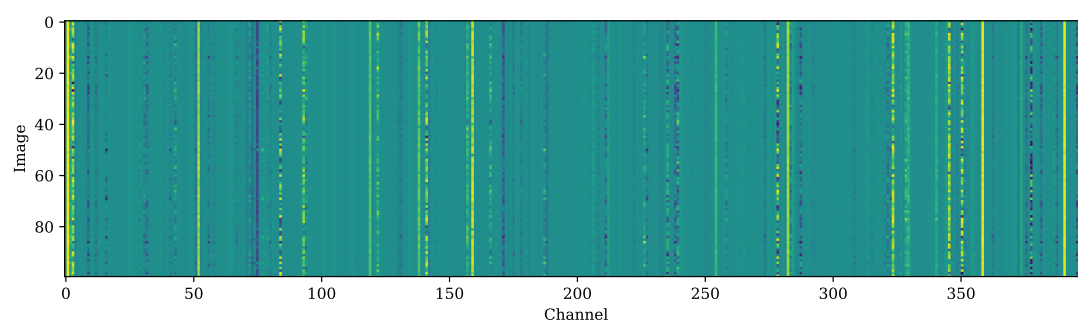


Figure 24. The attention values of different images from ResNet164-SE on CIFAR100. Zoom in for best view.

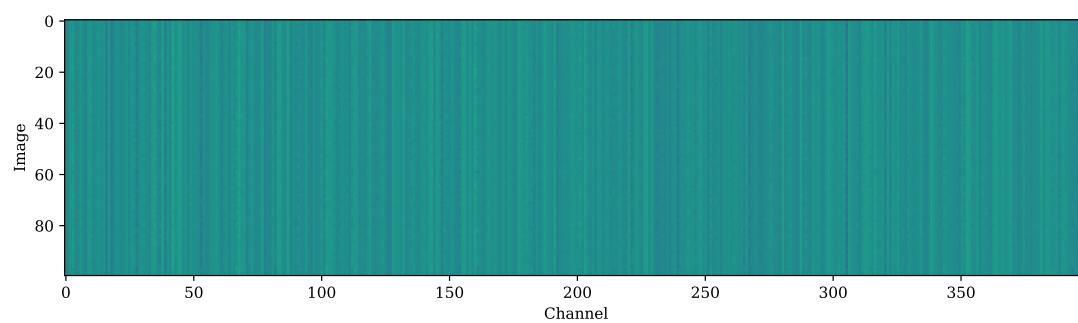


Figure 25. The attention values of different images from ResNet83-SE based on cosine learning rate on CIFAR100. Zoom in for best view.

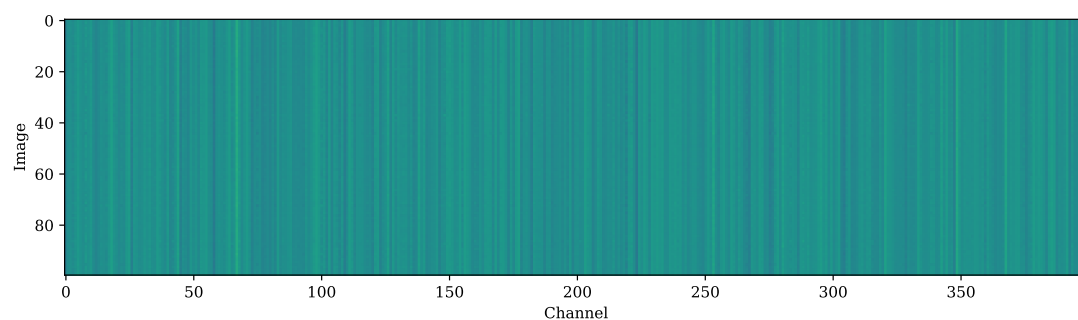


Figure 26. The attention values of different images from ResNet83-SE on STL10. Zoom in for best view.

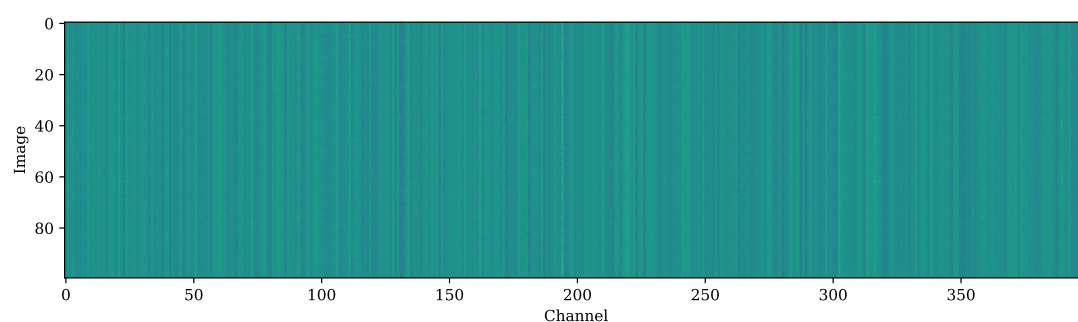


Figure 27. The attention values of different images from ResNet83-SE (weight decay: $2e-4$) on CIFAR100. Zoom in for best view.

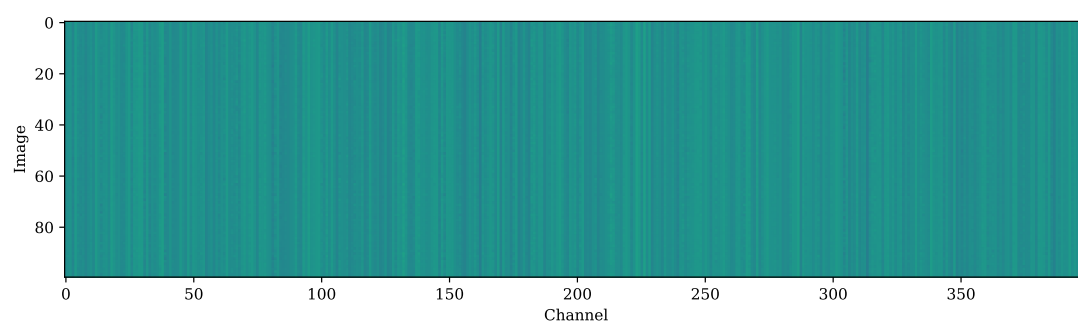


Figure 28. The attention values of different images from ResNet83-SE (weight decay: $3e-4$) on CIFAR100. Zoom in for best view.

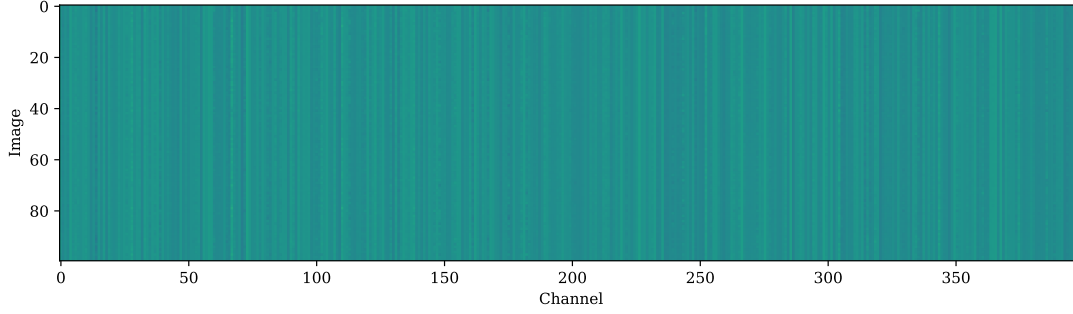


Figure 29. The attention values of different images from ResNet83-SE (weight decay: $4e-4$) on CIFAR100. Zoom in for best view.

I. Spatial and transformer-based ASR

As mentioned in our limitations, *Stripe Observation* as shown in Fig. 23, Fig. 24, Fig. 25, Fig. 26, Fig. 27, Fig. 28, and Fig. 29 does not hold for other types of attention, including spatial attention and transformer-based attention. In this section, we present visualizations of spatial attention and transformer-based attention and explore the performance of spatial and transformer-based ASR.

Spatial ASR. As shown in Fig. 30, we visualize the spatial attention values in CBAM. There exist variations in the spatial attention values for different images, and the overall distribution of the spatial attention values is scattered.

Transformer-based ASR. As shown in Fig. 31, we visualize the multi-head attention values in ViT. There exist variations in the multi-head attention values for different images, and the attention values for different images are related to the input image, for the reason that the highlighted parts in the visualization roughly correspond to the locations of the objects in the input images.

Comparisons. Table 15 presents the performance of spatial and transformer-based ASR. We observe that spatial ASR improves the performance of ResNet83 on STL10, but performs worse than vanilla ResNet83 on CIFAR100 and CIFAR10. Moreover, we find that the multi-head attention module is crucial for ViT, as ViT-Non multi-head attention performs significantly worse than vanilla ViT. Transformer-based ASR outperforms vanilla ViT on STL10, but underperforms on CIFAR100 and CIFAR10. Table 15 demonstrates the unstable performance of spatial and transformer-based ASR, indicating that it is preferable to use the spatial and transformer-based attention module directly.

Model	STL10		CIFAR100		CIFAR10	
	Top-1 acc.	Top-5 acc.	Top-1 acc.	Top-5 acc.	Top-1 acc.	Top-5 acc.
ResNet83	82.04	98.32	73.55	93.28	93.16	99.45
ResNet83-CBAM	83.62	98.98	73.24	93.64	93.31	99.76
ResNet83-ASR (CBAM, Spatial)	83.36	98.65	72.37	93.21	92.76	99.22
ViT-Non multi-head attention [†]	35.25	88.99	16.88	33.56	41.60	89.15
Vanilla ViT [†]	61.49	96.15	66.63	86.29	89.00	99.17
ViT-ASR (Multi-head attention) [†]	61.59	96.35	61.20	83.09	87.06	99.32

Table 15. The accuracy (%) of spatial and transformer-based ASR on STL10, CIFAR100, and CIFAR10. [†] All the experimental results of ViT. ASR (CBAM, Spatial) refers to the application of ASR only to the spatial attention module in CBAM. Vanilla ViT is a commonly used variant of ViT, ViT-Non multi-head attention refers to the removal of the multi-head attention modules in ViT, and ASR (Multi-head attention) refers to the application of ASR to the multi-head attention modules in ViT.

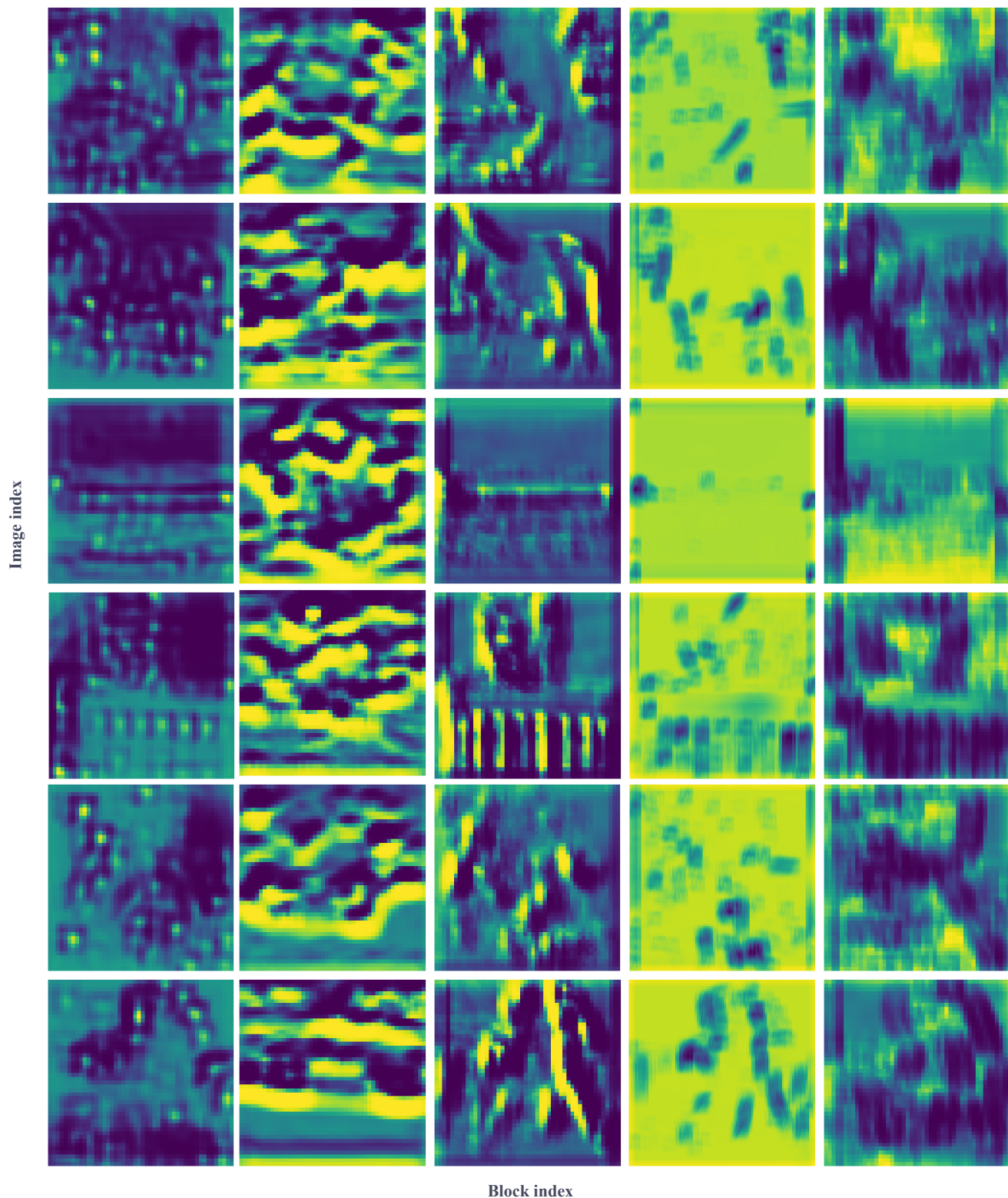


Figure 30. The visualization about the spatial attention from CBAM. We randomly select six images from STL10 and extract the spatial attention values of five blocks from ResNet83-CBAM. Each row in the visualization represents the spatial attention values of different blocks for the same image, while each column represents the spatial attention values of different images for the same block. Zoom in for best view.

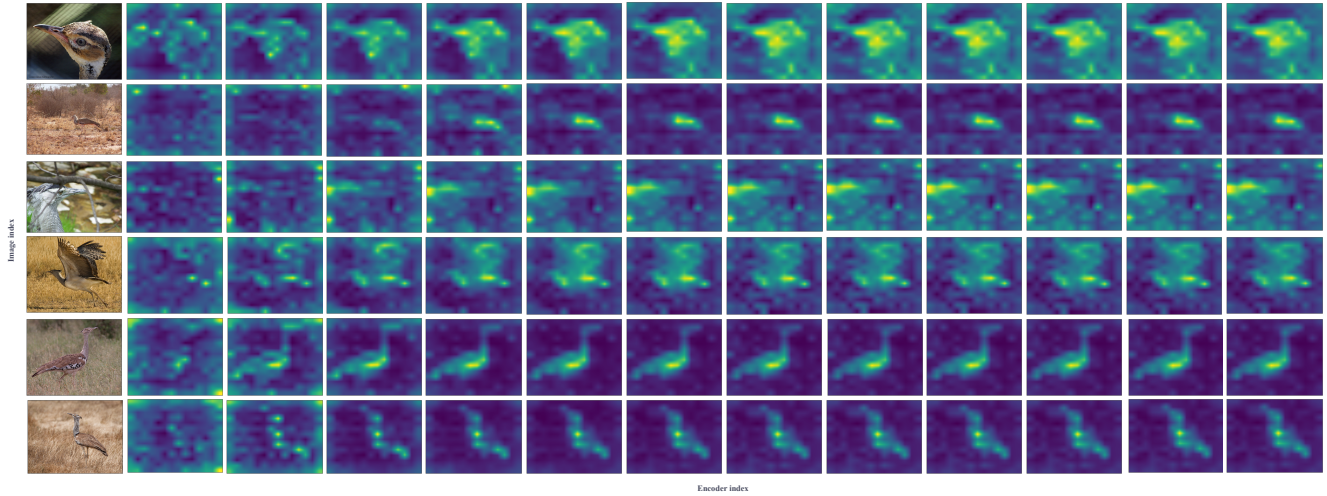


Figure 31. The visualization about the transformer-based attention from ViT. We utilize open-source ViT code and parameters (ViT-B_16-224), select six images from ImageNet and visualize the attention values of the 12 encoders in ViT's Transformer. Each row in the visualization represents the attention values of different encoders for the same image, while each column represents the attention values of different images for the same encoder. Zoom in for best view.